

# **Gasdermins mediate cellular release of mitochondrial DNA during pyroptosis and apoptosis**

Carlos de Torre-Minguela <sup>1\*</sup>, Ana I. Gómez <sup>1</sup>, Isabelle Couillin <sup>2</sup> and Pablo Pelegrín <sup>1,3\*</sup>

<sup>1</sup>Biomedical Research Institute of Murcia (IMIB-Arrixaca), Clinical University Hospital *Virgen de la Arrixaca*, 30120 Murcia, Spain.

<sup>2</sup>Experimental and Molecular Immunology and Neurogenetics, CNRS, UMR7355, University of Orleans, 45071 Orleans, France

<sup>3</sup>Department of Biochemistry and Molecular Biology B and Immunology, Faculty of Medicine, University of Murcia, 30120 Murcia, Spain.

**\*Corresponding authors:** Dr. Pablo Pelegrín. Edificio LAIB 4<sup>a</sup> Planta, Instituto Murciano de Investigación Biosanitaria (IMIB-Arrixaca). Carretera Buenavista s/n. 30120 El Palmar, Murcia, Spain. Phone number: +34 868885038; e-mail: pablo.pelegrin@imib.es

Dr. Carlos de Torre-Minguela. Edificio LAIB 4<sup>a</sup> Planta, Instituto Murciano de Investigación Biosanitaria (IMIB-Arrixaca). Carretera Buenavista s/n. 30120 El Palmar, Murcia, Spain. Phone number: +34868885034; e-mail: carlos.de3@um.es

**Running title:** Mitochondrial DNA release by gasdermins

**Keywords:** Pyroptosis / GSDMD / GSDME / mitochondrial DNA / Macrophages

**Total words count:** 5224 words excluded abstract, references and figure legends

**Figures:** 6 (Supplementary Figures: 4)

**List of nonstandard abbreviations:**

AMA: Antimycin A

BAK: B-cell lymphoma 2 antagonist killer

BAX: B-cell lymphoma 2 associated X

BID: BH3 interacting domain death agonist

BMDMs: Bone marrow derived macrophages

DAMP: Damage-associated molecular pattern

DAPI: 4',6-diamidino-2-phenylindole

DMSO: Dimethyl sulfoxide

GSDM: Gasdermin

GSDM<sup>NT</sup>: Amino-terminal of gasdermins

GSDMD<sup>NT</sup>: Amino-terminal of gasdermin D

HMGB1: High mobility group box 1

IL: Interleukin

LDH: Lactate dehydrogenase

LPS: Lipopolysaccharide

mtROS: Mitochondrial reactive oxygen species

MOMP: Permeabilization of the mitochondrial outer membrane

NLRP3: Nucleotide-binding oligomerization domain, leucine rich repeat and pyrin domain containing 3

SPN: Supernatant

tBid: Truncated-BID

TcdB: Toxin B of *Clostridium difficile*

TOMM20: Translocase of outer mitochondrial membrane 20

## **ABSTRACT**

Pyroptosis and intrinsic apoptosis are two forms of regulated cell death driven by active caspases where plasma membrane permeabilization is induced by gasdermin pores. Caspase-1 induces gasdermin D pore formation during pyroptosis whereas caspase-3 promotes gasdermin E pore formation during apoptosis. These two types of cell death are accompanied by mitochondrial outer membrane permeabilization due to BAK/BAX pore formation in the external membrane of mitochondria, and to some extent this complex also affects the inner mitochondrial membrane facilitating mitochondrial DNA relocalisation from the matrix to the cytosol. However, the detailed mechanism responsible for this process has not been investigated. Herein, we reported that gasdermin processing is required to induce mitochondrial DNA release from cells during pyroptosis and apoptosis. Gasdermin targeted at the plasma membrane promotes a fast mitochondrial collapse along with the initial accumulation of mitochondrial DNA in the cytosol and then facilitates the DNA's release from the cell when the plasma membrane ruptures. These findings demonstrate that gasdermin action has a critical effect on the plasma membrane and facilitates the release of mitochondrial DNA as a damage-associated molecular pattern.

## INTRODUCTION

Pyroptosis is a form of regulated cell death characterized by plasma membrane rupture mediated by gasdermin D (GSDMD) pores and the release of inflammatory intracellular molecules (1, 2). This type of cell death is triggered by pathogens or by perturbances on cell homeostasis that inducing canonical inflammasome dependent caspase-1 activation or non-canonical activation of murine caspase-11 or human caspase-4/-5 (3). Caspase-1, -4, -5 and -11 proteolytically process GSDMD in their interdomain loop thus generating an amino-terminal GSDMD (GSDMD<sup>NT</sup>) that binds to the plasma membrane and generates oligomeric pores responsible for plasma membrane permeabilization (4–6). A similar process may also occur during the execution of other types of cell death, like apoptosis, where caspase-3 cleavages GSDME, another member of the gasdermin protein family, and GSDME<sup>NT</sup> forms pores in the plasma membrane (7, 8). In addition, active caspase-3 inactivates GSDMD by processing in the middle of GSDMD<sup>NT</sup> (9). Both types of cell death involve the permeabilization of the mitochondrial outer membrane (MOMP), this being an initial step of the intrinsic apoptotic pathway. MOMP occurs through the oligomerization of B-cell lymphoma 2 associated X (BAX) and B-cell lymphoma 2 antagonist killer (BAK) proteins in the mitochondrial outer membrane, which forms pores and allows the release of cytochrome C to the cytosol. Cytosolic cytochrome C facilitates the assembly of the apoptosome, thus leading to the activation of caspase-9 and the subsequent activation of caspase-3 (10, 11). BAX/BAK oligomerization is initiated when BH3 interacting domain death agonist (BID) is processed by caspase-1 and -8 (12, 13).

Even though plasma membrane permeabilization is the most studied effect of amino-terminal gasdermin (GSDM<sup>NT</sup>) pores, cell organelle membranes have also been recently described as targets of these proteins. In neutrophils, the main targets of GSDMD<sup>NT</sup> are azurophilic granules, the nuclei and LC3<sup>+</sup> autophagosomes, thus allowing the release of IL-1 $\beta$  in the absence of plasma membrane rupture and inducing neutrophil death by NETosis (14, 15). GSDMD<sup>NT</sup> and GSDME<sup>NT</sup> can also form pores in the external membrane of mitochondria and thus facilitate the release of cytochrome C (16). Therefore, during pyroptosis and apoptosis, different pathways can target the mitochondria.

Super-resolution imaging has shown that BAK/BAX pores in the external membrane of mitochondria facilitate mitochondrial DNA release during intrinsic apoptosis (17, 18). However, none of these

studies considered the role of GSDM<sup>NT</sup> and plasma membrane permeabilization in this process. In the current study, we describe the inhibition of mitochondrial DNA release into the cytosol in *Gsdmd*-deficient macrophages during the canonical induction of pyroptosis, despite mitochondrial damage by the activation of caspase-1. The MOMP generated by caspase-1 activation is not enough to induce morphological changes in the mitochondrial network in the absence of GSDM<sup>NT</sup> and plasma membrane permeabilization. GSDM<sup>NT</sup> influenced plasma membrane permeabilization and mitochondrial DNA release during pyroptosis and intrinsic apoptosis, both of which were dependent on GSDMD<sup>NT</sup> and GSDME<sup>NT</sup> respectively. The treatment of macrophages with punicalagin, a compound that blocks plasma membrane permeabilization during pyroptosis (19), inhibits mitochondrial DNA release from the cells during pyroptosis, whereas the presence of glycine, a cytoprotector that prevents plasma membrane rupture but allows their permeabilization (20), produces an accumulation of mitochondrial DNA over time in the cytosol. Therefore, our study demonstrates that GSDMs are critical to facilitating the fragmentation of the mitochondrial network and the release of mitochondrial DNA during pyroptosis and apoptosis by plasma membrane permeabilization.

## MATERIALS AND METHODS

### Reagents, plasmids and cells.

Key reagents and their sources were as follows: ATP, antimycin A (AMA), DAPI, digitonin, *Escherichia coli* LPS serotype 055:B5, glycine, MitoTEMPO, nigericin sodium salt and staurosporine were from Sigma-Aldrich (Spain). Toxin B was from *Clostridium difficile* (ENZO Life Science, USA). HPLC-purified punicalagin was from Probelte Biotechnology S.L. Pluronic acid was from Merck-Millipore (Spain). MitoSOX™ Red and Yo-Pro-1 iodide were from Thermo Fisher Scientific (USA). The composition of the physiological buffer (ET buffer) used in all experiments to stimulate macrophages was (in mM): 147 NaCl, 10 HEPES, 13 D-glucose, 2 KCl, 2 CaCl<sub>2</sub>, and 1 MgCl<sub>2</sub>; pH 7.4.

HEK293T cells (ATCC CRL-11268) were cultured in DMEM:F-12 media (1:1; Lonza) supplemented with 10% of fetal calf serum (Life Technologies, Spain) and 2 mM Glutamax (Life Technologies, Madrid, Spain). For transfection experiments, HEK293T cells were seeded overnight over coverslips on 24-well plates at a density of  $35 \times 10^3$  cells per well. The next day, cells were transfected with 250 ng of plasmid DNA using Lipofectamine 2000 (2  $\mu$ L/mL) as per the manufacturer's indications (Invitrogen, Spain) in 0.3 mL of Opti-MEM™ (Fischer Scientific, Spain) per well. Plasmid coding for human full length GSDMD and N-terminal GSDMD (1-275) were inserted in modified pCS2-3xFlag as described (4) and human N-terminal GSDME (1-270) were inserted in pEGFPN1 as described, with a stop codon to avoid EGFP expression (7).

### Mice.

C57BL/6 wild type mice were purchased from Harlan. P2X7 receptor-deficient (*P2rx7<sup>-/-</sup>*) (21), NLRP3-deficient (*Nlrp3<sup>-/-</sup>*) (22), double caspase-1/11-deficient (*Casp1/11<sup>-/-</sup>*) (23) and GSDMD-deficient (*Gsdmd<sup>-/-</sup>*) mice were all in C57BL/6 background. For all experiments, mice between 8-10 weeks of age bred under SPF conditions were used in accordance with the Spanish national (RD 1201/2005 and Law 32/2007) and EU (86/609/EEC and 2010/63/EU) legislation. No procedure was performed on the animals as they were sacrificed for tissue (bone marrow) and the animal

experimentation committee of the University of Murcia approved the use of the animals with reference CEEA 5/2014.

#### **Differentiation and *in vitro* stimulation of macrophages from mouse bone marrow precursors.**

Bone marrow derived macrophages (BMDMs) were obtained as described (24). Cells were primed 4 h with LPS at 10 ng/ml then washed three times with physiological buffer before being added with the treatments specified in the figure legends in either physiological buffer or Opti-MEM media (for staurosporin treatments). In some experiments, stimulation with nigericin and punicalagin was stopped after 15 min, cells were washed twice and incubated for further 10 min in physiological buffer at 37°C before cell fixation. Supernatants were collected and clarified by centrifugation and stored at -80°C. Cells were ruptured immediately in lysis buffer (50 mM Tris-HCl pH8.0, 150 mM NaCl, 2% Triton X-100) supplemented with 100 µl/ml of protease inhibitor mixture (Sigma) for 30 min on ice and then cell debris was removed by centrifugation at 16,000g for 15min at 4 °C.

#### **Lactate dehydrogenase (LDH) determination.**

Presence of LDH in cell-free supernatants was used as marker for cell death and was measured using the Cytotoxicity Detection kit (Roche, Barcelona, Spain) following the manufacturer's instructions and read in a Synergy Mx plate reader (BioTek, USA). Values were expressed as a percentage of total cellular LDH content.

#### **Enrichment of cytosolic and organelle fractions.**

To determine cytochrome C release from mitochondria, cytosolic and organelle fractions were enriched from  $2 \times 10^6$  cells per sample primed with LPS and exposed to different stimuli for various times or left untreated as indicated in the figure legends. Cells were harvested in 100 µl phosphate-buffered saline and lysed by adding 100 µl of a digitonin (17.5 µg/ml) /sucrose (500 mM) solution under vigorous vortexing for 30 seconds. Cytosolic fractions were quickly isolated from organelles and cell debris by centrifugation at 14,000g for 5 min at 4°C. As a reference for the cytochrome C content of the cells, organelle-comprising fractions of cells were lysed in buffer (50 mM Tris-HCl

pH8.0, 150 mM NaCl, 2% Triton X-100) supplemented with 100 µl/ml of protease inhibitor mixture for 30 min on ice and then separated from cell debris by centrifugation at 16,000g for 15min at 4 °C. Mitochondrial fractions were enriched by ultracentrifugation following the protocol described (25) or by based-antibodies method following the protocol described in the Mitochondria Isolation Kit for mouse tissue (Miltenyi Biotech) to determine GSDMD<sup>NT</sup> in this organelle.

### **Western blots.**

Cells lysates, organelle fractions and precipitated cell-free supernatants were resolved in 4–12% precast Criterion polyacrylamide gels (Biorad) and transferred to nitrocellulose membranes (Biorad) by electroblotting, as described in (26). Membranes were probed with different antibodies: anti-NLRP3 mouse monoclonal (Cryo-2, AG-20B-0014, Adipogen), anti-cytochrome c mouse monoclonal (7H8.2C12, ab13575, Abcam), anti-BID rat monoclonal (#91508, MAB860, R&D), anti-alpha tubulin rabbit polyclonal (ab4074, Abcam); anti-cleaved caspase-3 rabbit polyclonal (#9661, Cell signalling), horseradish peroxidase-anti-β-actin (C4; sc-47778HRP, Santa Cruz), anti-Flag M2 mouse monoclonal (Clone M2, F3165, Sigma-Aldrich), anti-caspase-1 p10 rabbit polyclonal (M-20, sc-514, Santa Cruz), anti-Tomm20 rabbit monoclonal (EPR15581-54, ab186735, Abcam), anti-GSDMD rabbit monoclonal (EPR19828, ab209845, Abcam) and anti-GSDME rabbit monoclonal (EPR19859, ab215191, Abcam).

### **ELISA assay.**

Individual culture cell-free supernatants were collected, clarified by centrifugation and the concentration of IL-1β was tested by ELISA following the manufacturer's instructions (R&D Systems). HMGB1 was also tested in cell-free supernatants by ELISA following the manufacturer's instructions (IBL International).

### **MitoSOX™ Red and YoPro-1 uptake assays.**

Superoxide production was measured using MitoSOX™ Red fluorescent probe (Thermo Fisher Scientific, USA) as described in (27). Briefly, BMDMs grown in black multiwell plates (10<sup>5</sup> cells per well) were primed or not for 4h with LPS at 10 ng/ml. Cells were then washed twice with physiological

buffer before being incubated for 10 min at 37 °C with 5µM of MitoSOX™ Red. After incubation, cells were washed twice before adding different stimuli or being left untreated as indicated in the figure legends. The fluorescence was monitored in physiological buffer by an automatic fluorescence plate reader (Synergy Mx; BioTek) for 60 min at 1 min intervals at a wavelength excitation of 510 nm (bandwidth:9nm) and a wavelength emission of 595 nm (bandwidth:20 nm).

MitoSOX™ Red and YoPro-1 iodide fluorescence was parallel monitored in physiological buffer by an automatic fluorescence plate reader (Synergy Mx; BioTek, USA) every 20 s for 50 min at 37 °C before and after the addition of nigericin or digitonin at the concentration indicated in the figure legends. Fluorescence of DNA-bound YoPro-1 was measured at 485±9 nm excitation and 515±9 nm emission and MitoSOX™ Red at a wavelength excitation of 510±9 nm and a wavelength emission of 595±20 nm. The assay was performed in the same plate but with different wells for MitoSOX™ Red and YoPro-1.

#### **Mitochondrial DNA release assay.**

Mouse mitochondrial DNA was isolated from the supernatant or cytosolic fraction of different genotypes of BMDM stimulated as described in the figures using a DNeasy Blood & Tissue Kit (QIAGEN). The same kit was also used to isolate human mitochondrial DNA from the supernatant of transfected HEK293T cells. The standard mouse mitochondrial DNA was obtained from mitochondria isolated from BMDM C57BL/6 using the Mitochondria Isolation Kit for mouse tissue (Miltenyi Biotec, Bergisch Gladbach, Germany) as described by the manufacturer. The standard human mitochondrial DNA was obtained from mitochondria isolated from HEK293T cells using the protocol described by (25). The standard curve of mitochondrial DNA was obtained in each assay for absolute quantification of mitochondrial DNA. Quantitative PCR was employed to measure mitochondrial DNA using TB Green™ Premix Ex Taq (TAKARA BIO INC, Japan) in an iQ5 Real-Time PCR System (Bio-Rad). The following primer was used: mouse mitochondrial cytochrome c oxidase I (F: 5'-GCCCCAGATATAGCATTCCC-3' and R: 5'-GTTCATCCTGTTCTGCTCC-3'); human mitochondrial cytochrome b (F: 5'-CCCCACAAACCCATTACTAAACCCA-3' and R 5'-TTCATCATGCGGAGATGTTGGATGG-3').

### **Microscopy.**

BMDMs were seeded on coverslips. After treatment, the cells were fixed for 15 min at room temperature with 4% formaldehyde in PBS, and were then washed six times with PBS. Nonspecific binding in cells was blocked with 0.5% bovine serum albumin (Sigma) and cells were permeabilized for 40 min at room temperature with 0.15% TritonX100 (Sigma) in PBS before incubation for 2 h at room temperature with the primary antibody anti-Tomm20 rabbit monoclonal IgG (1:500 dilution; EPR15581-54, ab186735, Abcam) or anti-DNA mouse monoclonal IgM (1:10 dilution AC-30-10, CBL186, Merck). Cells were washed with PBS and were then incubated for 1 h at room temperature with the appropriate fluorescence-conjugated secondary antibody (1:800 dilution; Alexa Fluor 488 donkey anti-rabbit IgG, Molecular Probes by Life Technology, Madrid, Spain). Alexa Fluor 647 goat anti-mouse IgM mu chain (Abcam, Cambridge, UK) was then rinsed in PBS and incubated for 10 min with DAPI (1  $\mu$ g/ml). All coverslips were mounted on slides with Fluorescence mounting solution (DAKO). Images were acquired with a Nikon Eclipse Ti microscope equipped with a  $\times$  40 S Plan Fluor objective (numerical aperture, 0.6) and a 60  $\times$  /0.60S Plan Fluor objective and a digital Sight DS-QiMc camera (Nikon, Tokyo, Japan) with a Z optical spacing of 0.4  $\mu$ m and 387-nm/447-nm, 472-nm/520-nm, 543-nm/593-nm and 650-nm/668-nm filter sets (Semrock). Deconvolved maximum-intensity projection of images was achieved with ImageJ software and a 3D parallel iterative deconvolution plugin (US National Institutes of Health).

### **Statistical analysis.**

All data are shown as mean values and the error bars represent standard error from the number of independent assays indicated in the figure legend. For two-group comparisons, Mann-Whitney test was applied using Prism software (Graph-Pad Software, Inc.).  $p$  value is indicated as \*\*\* $p$  < 0.001; \*\* $p$  > 0.001 < 0.01; \* $p$  > 0.01 < 0.05;  $p$  > 0.05 not significant (ns).

## RESULTS

### **NLRP3 inflammasome activation induces GSDMD-dependent mitochondrial network fragmentation**

NLRP3 inflammasome activation with ATP or nigericin induced the generation of truncated-BID (tBid) in macrophages and tBid generation is dependent on caspase-1 (Fig. 1A). However, we observed that GSDMD deficiency did not affect tBid generation (Fig. 1A). As a control for GSDMD function, we found that the release of interleukin (IL)-1 $\beta$  and lactate dehydrogenase (LDH) after NLRP3 inflammasome activation decreased in both *Gsdmd*<sup>-/-</sup> and *Casp1/11*<sup>-/-</sup> macrophages (Supplementary Fig. S1A,B). Detection of LDH enzymatic activity in supernatant suggests a severe rupture of the plasma membrane in this cellular model because LDH (tetramer complex) is not able to pass through GSDMD pores (28, 29). We then found that tBid could be damaging mitochondria because we detected the presence of cytochrome C in the enriched cytosol after NLRP3 inflammasome activation in wild type and also in *Gsdmd*<sup>-/-</sup> macrophages, but not in *Casp1/11*<sup>-/-</sup> macrophages (Fig. 1B). The outer membrane mitochondrial integral protein TOMM20 and the cytosolic  $\alpha$ -tubulin protein show that the organelle enriched fraction was minimally contaminated with cytosol and vice versa (Supplementary Fig. S1C). However, we cannot rule out the presence of other organelles in cytosolic fractions or the possibility of obtaining pure fractions with the protocol used. These results confirm the presence of MOMP induced by caspase-1 activation independently of GSDMD<sup>NT</sup> generation, revealing that caspase-1 could simultaneously induce different signaling pathways associated with mitochondrial damage (13).

In agreement with a recent study (16), we detected GSDMD<sup>NT</sup> in the enriched organelle fraction (Fig. 1B) and specifically in the enriched mitochondrial fractions obtained from macrophages treated with ATP or nigericin using either ultracentrifugation or an antibody-based method to enrich mitochondria (Supplementary Fig. S1D,E). To examine whether GSDMD promote mitochondrial damage beyond BAX/BAK MOMP, we studied mitochondrial morphology and mitochondrial network by staining with the mitochondrial marker TOMM20. Activation of NLRP3 inflammasome by ATP or nigericin resulted in characteristic morphological features of pyroptotic cells such as the condensation of the nucleus (30), and also in a fragmentation of the mitochondrial network (Fig. 1C and Supplementary Fig. S1F),

where sections of the mitochondrial network appeared rounded ( $64.34 \pm 2.18$  % of cells with rounded mitochondria). Mitochondrial sphericity was not present in *Casp1/11*<sup>-/-</sup> or *Gsdmd*<sup>-/-</sup> macrophages after NLRP3 inflammasome stimulation (Fig. 1C and Supplementary Fig. S1F), even though GSDMD deficiency was not preventing cytochrome C release (Fig. 1B). This suggests that caspase-1 induced-MOMP is not reflected in morphological changes to the mitochondrial network.

### **GSDMD induces mitochondrial DNA release after NLRP3 inflammasome activation**

Loss of mitochondrial membrane integrity is usually associated with the generation of mitochondrial reactive oxygen species (mtROS) (31). We used MitoSOX as a marker of mitochondrial superoxide production to test whether mitochondrial damage dependent on caspase-1 activation is involved in mtROS production. As expected, MitoSOX fluorescence increased after ATP or nigericin treatment of wild type macrophages, but did not in either *Casp1/11*<sup>-/-</sup> or *Gsdmd*<sup>-/-</sup> macrophages (Fig. 2A). This suggests that the association of MitoSOX fluorescence increases with the activity of caspase-1 and GSDMD. As a control, treatment with antimycin A, a mitochondrial complex III inhibitor, showed an increase in MitoSOX fluorescence independent from caspase-1 and GSDMD (Fig. 2A). Similarly, the treatment of unprimed macrophages with ATP or nigericin failed to increase MitoSOX fluorescence (Supplementary Fig. S2A) and this is to be expected because NLRP3 priming is essential for caspase-1 activation (32) and the subsequent induction of mitochondrial damage. Antimycin A increased MitoSOX fluorescence in both primed (Figure 2A) and non-primed macrophages (Supplementary Fig. S2A), but failed to induce cytochrome C release to the cytosol (Fig. 1B). The use of the mitochondrial-targeted antioxidant MitoTEMPO reduced the increase in MitoSOX fluorescence during nigericin stimulation (Supplementary Fig. S2B), showing that MitoSOX fluorescence increase may not depend only on mtROS caused by caspase-1 mitochondrial damage. In fact, given that cytochrome c was released from mitochondria in *Gsdmd*<sup>-/-</sup> macrophages, and cytochrome c release has been associated with increased superoxide production (33), we next localized MitoSOX cellular staining and found that it was not only associated with mitochondria, but also with cytosol and nuclei (Supplementary Fig. S2C). MitoSOX is a lipophilic fluorescent molecule with a positively charged moiety that allows it to be located within the mitochondrial matrix for mtROS

detection (34) and also allows it to interact with nucleic acids to increase its fluorescence (35, 36). Therefore, we hypothesized that increased MitoSOX fluorescence could also be due to the presence of nucleic acids such as mitochondrial DNA in the cytosol during GSDMD-mediated cell death. To test this hypothesis, we specifically measured mitochondrial DNA in the cytosolic fraction and found that the activation of NLRP3 induced a significant increase in mitochondrial DNA in the cytosol dependent on both caspase-1 and GSDMD (Fig. 2B), suggesting that GSDMD plays a role in the release of mitochondrial DNA from damaged mitochondria. In addition, treatment with nigericin induced the presence of mitochondrial DNA-containing nucleoids associated with rounded mitochondria during mitochondrial network fragmentation (Fig. 2C). This morphology has been previously found during apoptosis-induced mitochondrial DNA release processes (17, 18). Furthermore, NLRP3 stimulation also resulted in a GSDMD-mediated release of mitochondrial DNA in cellular supernatants (Fig. 2D). These results confirm that mitochondrial DNA relocalisation to the cytoplasm during pyroptosis requires caspase-1 and GSDMD, with caspase-1-induced MOMP being insufficient for this process.

### **Pyrin inflammasome activation and GSDMD<sup>NT</sup> induce mitochondrial DNA release**

To investigate if the activation of other inflammasomes beyond NLRP3 could also promote mitochondrial DNA release, we triggered in *Nlrp3*<sup>-/-</sup> macrophages the pyrin inflammasome with the toxin B of *Clostridium difficile* (TcdB). The use of NLRP3-deficient macrophages ensured that this inflammasome would not be activated during the initial steps of pyroptosis. TcdB induced the generation of tBid and GSDMD<sup>NT</sup> (Fig. 3A) in parallel with the release of IL-1 $\beta$  and LDH (Fig. 3B). As with NLRP3 activation, pyrin induction also resulted in a mitochondrial network fragmentation dependent on caspase-1 (Fig. 3C). Importantly, mitochondrial DNA was also released during pyrin inflammasome-induced pyroptosis (Fig. 3D).

To study if GSDMD<sup>NT</sup> by itself was able to induce mitochondrial damage independently of caspase-1 and inflammasome activation, we expressed GSDMD<sup>NT</sup> in HEK293T cells (Supplementary Fig. S3A). The expression of GSDMD<sup>NT</sup> also induced mitochondrial network fragmentation and a condensation of the nucleus (Fig. 3E), suggesting that these cells present pyroptotic features. Release of HMGB1

in the GSDMD<sup>NT</sup>-expressing cells (Fig. 3F) also confirmed cell permeabilization. In cells expressing GSDMD<sup>NT</sup>, mitochondrial DNA significantly increased in the supernatant (Fig. 3F). Therefore, GSDMD<sup>NT</sup> is able to directly facilitate mitochondrial network fragmentation and the release of mitochondrial DNA, independently of the stimulation of inflammasome or caspase-1 induced MOMP.

### **Mitochondrial DNA release is also promoted by GSDME<sup>NT</sup>**

We then aimed to investigate if other activated GSDMs could also be promoting mitochondrial DNA release, so we stimulated macrophages with staurosporine, a nonselective inhibitor of several kinases that induced caspase-3 activation through intrinsic apoptosis independently of BAX/BAK pores (37). Caspase-3 is able to induce cleavage of GSDME, switching apoptosis into pyroptosis-like cell death (7). However, since treatment of macrophages with staurosporin also induces caspase-1 activation (38), the use of wild type macrophages would make it difficult to differentiate the potential contribution of GSDME to mitochondrial DNA release induced by staurosporine; therefore, we used non-primed *Casp1/11*<sup>-/-</sup> macrophages. In this cellular context, we found caspase-3 activation and GSDME processing after 4 h of staurosporine treatment (Fig. 4A), as has been described (7, 8, 16). In addition, in this context, caspase-1 and GSDMD activation was avoided (Fig. 4A).

We then aimed to investigate the role of GSDME processing in plasma membrane permeabilization by using the DNA staining YoPro-1, which is cell impermeant and enters the cell on permeabilization of the plasma membrane. Cellular YoPro-1 uptake experiments showed efficient cell permeabilization in LPS-primed macrophages after 30 minutes of nigericin treatment and in non-primed *Casp1/11*<sup>-/-</sup> macrophages treated with staurosporine for 4 h (Supplementary Fig. S3B). In parallel, we observed that *Casp1/11*<sup>-/-</sup> macrophages treated for 4 h with staurosporine presented other features of pyroptosis and membrane permeabilization such as a significant release of LDH and HMGB1 (Fig. 4B), similar to that which was observed in parallel experiments using wild type macrophages and in which GSDMD pyroptosis was induced (Fig. 4B). Also, staurosporine treated macrophages showed the same mitochondrial network fragmentation detected during GSDMD-mediated pyroptosis (Fig. 4C) and significant release of mitochondrial DNA (Fig. 4D), thus supporting the idea that plasma membrane permeabilization produced by GSDME<sup>NT</sup> could also facilitate mitochondrial DNA release.

To confirm the role of GSDME<sup>NT</sup> in inducing mitochondrial DNA release, we expressed GSDME<sup>NT</sup> in HEK293T cells (Supplementary Fig. S3C). GSDME<sup>NT</sup> induced a significant release of HMGB1 in the supernatant (Fig. 4E), confirming effective plasma membrane permeabilization. Also, GSDME<sup>NT</sup> expression induced mitochondrial network fragmentation (Fig. 4F) and significant mitochondrial DNA release (Fig. 4G). These data show that GSDME-mediated pore formation induces the release of damage-associated molecular patterns (DAMPs), not only HMGB1, but also mitochondrial DNA. This process could be triggered by GSDME during intrinsic apoptosis in macrophages.

### **GSDMD promotes mitochondrial DNA relocalisation to the cytosol in the absence of cell lysis**

The loss of plasma membrane integrity and pyroptosis downstream from caspase-1 activation can be prevented by glycine, a cytoprotectant that allows GSDMD pore formation but prevents cell lysis (29). Parallel increase of YoPro-1 uptake and MitoSOX fluorescence was found in LPS-primed macrophages treated with nigericin in the presence of glycine (Fig. 5A), suggesting potential mitochondrial damage in parallel to plasma membrane permeabilization and in the absence of cell death, as the use of glycine prevented LDH release, but not IL-1 $\beta$  release (Fig. 5B). In this situation, glycine was not able to prevent nigericin-induced release of cytochrome C to the cytosol (Fig. 5C), nor mitochondrial network fragmentation (Fig. 5D). However, we detected a significantly lower amount of mitochondrial DNA released in the supernatant from cells treated with glycine (Fig. 5E), whereas the amount of mitochondrial DNA detected in the cytosolic fraction accumulated over-time in glycine treated cells (Fig. 5E). Therefore, pyroptotic cell lysis with a severe rupture of the plasma membrane is required for cellular mitochondrial DNA release, but not for mitochondrial damage and DNA relocalisation to the cytosol.

### **GSDMD<sup>NT</sup> plasma membrane pore activity is required for mitochondrial damage**

In order to determine if GSDMD-induced plasma membrane pore formation could critically contribute to mitochondrial damage and DNA release, in addition to direct GSDMD<sup>NT</sup> permeabilization of the mitochondria, we used punicalagin as a polyphenolic compound able to impair plasma membrane pore formation and IL-1 $\beta$  release after caspase-1 activation (19). Here, we found that after NLRP3

activation, punicalagin did not affect GSDMD<sup>NT</sup> generation (Fig. 6A) nor the MOMP because cytochrome c was found in cytosolic enriched fractions (Fig. S4A). However, as expected, it did prevent YoPro-1 uptake (Fig. 6B), suggesting the inhibition of plasma membrane GSDMD<sup>NT</sup> pore activity. Likewise, cell death and the release of mitochondrial DNA to cell supernatants was also blocked by punicalagin (Fig. 6C). The presence of punicalagin, despite the presence of intracellular GSDMD<sup>NT</sup>, also protected mitochondria network structure and prevented the increase of MitoSOX fluorescence upon nigericin treatment (Fig. 6D and E). Punicalagin washout quickly resulted in a mitochondrial sphericity, mitochondrial network fragmentation and intense staining of released mitochondrial DNA (Fig. 6D). These data suggest that pores of GSDMD<sup>NT</sup> in the plasma membrane could be contributing to mitochondrial damage and mitochondrial DNA relocalisation to the cytosol. To further support this hypothesis, we used melittin, a bee venom toxin, to form pores in the plasma membrane (39). Melittin was able to induce an alteration in the mitochondria (Supplementary Fig. S4B). In addition, a low concentration of digitonin, which allows the analysis of mitochondrial function *in situ* (40, 41), was able to induce YoPro-1 uptake with a parallel increase in MitoSOX fluorescence (Supplementary Fig. S4C). Furthermore, plasma membrane permeabilization with digitonin induced a similar mitochondrial network fragmentation to the one found during pyroptosis (Supplementary Fig. S4D) and mitochondrial DNA release (Supplementary Fig. S4E). Taken together, our study demonstrates that plasma membrane permeabilization by GSDMD<sup>NT</sup> contributes to the release of mitochondrial DNA in two steps: an initial step that induces the relocalisation to the cytosol during fragmentation of the mitochondrial network, and a second step that facilitates its cellular release after severe plasma membrane destabilization during pyroptosis and intrinsic apoptosis.

## DISCUSSION

In the present study, we provide evidence of the important role played by GSDMs in inducing plasma membrane permeabilization and cellular mitochondrial DNA release during two forms of regulated cell death, pyroptosis and intrinsic apoptosis, which confirms GSDMs as a common pathway for the cellular secretion of DAMPs.

Extracellular mitochondrial DNA is a well-recognized DAMP which participates in the inflammatory response by activating neutrophils and endothelial cells (42–44) and is also found circulating in plasma from patients with different pathologies. Here we found that GSDM processing during pyroptosis or apoptosis helps to induce the release of mitochondrial DNA to the extracellular space, thus suggesting a potential pathophysiological role for GSDMs in arthritis, type 2 diabetes, and cardiovascular or lupus-like diseases (45–48). In addition, cellular mitochondrial DNA release is accompanied by an initial relocation to the cytosol that activates the production of type I interferon through the cGAS-STING signaling pathway, although the subsequent downstream activation of caspases and GSDMD pores suppresses this immunological response (44, 49, 50). It might be possible that other GSDMs that are less active in the plasma membrane and activated in the absence of caspases (1, 2) amplify this pathway. Our study also supports the possibility that GSDMD<sup>NT</sup> might impair intracellular cGAS-STING, as has been proposed (51) by facilitating the release of mitochondrial DNA from the cytosol to the extracellular medium and decreasing the accumulation of cytosolic DNA during effective pyroptotic cell lysis.

We show that caspase-1 activation could damage mitochondria by different pathways, one being the cleavage of BID to induce the release of MOMP and cytochrome C into the cytosol (12, 13). Our data show caspase-1-dependent BID cleavage after activation of NLRP3 and pyrin inflammasome in macrophages and demonstrate that MOMP is induced independently of GSDMD activation and pore formation. However, we identify GSDMD as a critical player in severe fragmentation of the mitochondrial network after caspase-1 activation, where the mitochondrial network appears rounded instead of filamentous. We do not observe these morphological changes in the mitochondrial network of GSDMD-deficient macrophages despite observing BID cleavage and cytosolic cytochrome C release upon caspase-1 activation, indicating that GSDMD would contribute to the collapse of the

mitochondrial network. It has been proposed that MOMP induced by BAX/BAK pores would facilitate the release of mitochondrial DNA into the cytosol (17, 18); however, in those studies caspases are routinely blocked by a pan-caspase inhibitor. In contrast, our data show the inhibition of mitochondrial DNA release into the cytosol in the absence of GSDMD despite observing BID cleavage after caspase-1 activation. It is unclear whether the stimulation time on *Gsdmd*<sup>-/-</sup> macrophages was insufficient to detect mitochondrial DNA relocalisation due to MOMP in the presence of active caspase-1; however, our results indicate that GSDMD contribute to the acceleration and facilitation of mitochondrial DNA relocalisation during pyroptosis where active caspases are present.

Recent studies have shown that other members of the GSDM protein family lead to plasma membrane permeabilization after proteolytic processing by active caspases. Specifically, GSDME is processed by caspase-3, thus switching apoptosis to a pyroptosis-like phenotype and leading to plasma membrane permeabilization and facilitating the release of DAMPs (7, 8). Our data suggest that GSDME<sup>NT</sup> facilitates the cellular release of HMGB1 and mitochondrial DNA, as well as inducing mitochondrial network fragmentation in two cellular models independently of caspase-1 activation. This is in agreement with recent work showing GSDME<sup>NT</sup> targeting the mitochondria and inducing cytochrome C release (16), suggesting that the release of mitochondrial DAMPs could be a general consequence of the action of GSDM<sup>NT</sup>. However, our data suggest that the GSDM<sup>NT</sup> permeabilization of the plasma membrane could also be a key step for mitochondrial damage.

Plasma membrane permeabilization induced by pore-forming proteins or toxins generates ruptures in plasma membrane because of the release of large intracellular molecules such as the tetrameric LDH enzyme, which cannot directly permeate through the formed pores (19, 28, 29). The lytic cell death produced by pneumolysin, a bacterial toxin produced by *Streptococcus pneumoniae*, activates the immunological system through mitochondrial DNA release from epithelial cells and also produces morphological alterations in the mitochondrial network (52); likewise in the present study we also show that another pore-forming toxin, the bee venom peptide melittin, induces mitochondrial network fragmentation. In line with these results and with the data we obtained after using GSDMs to induce plasma membrane permeabilization, we observed the same phenomena of mitochondrial network fragmentation induced by plasma membrane permeabilization with low concentrations of digitonin, a

treatment that allows the analysis of mitochondrial function *in situ* without the isolation of organelles (40). Therefore, the changes in ionic homeostasis produced by plasma membrane permeabilization accompanied by ruptures in the plasma membrane (induced either by GSDM pores or non-selective pores) might contribute to mitochondrial collapse and thus encourage the relocalisation of mitochondrial DNA to the cytosol. The use of the cytoprotective agent glycine while GSDMD<sup>NT</sup> was generated by activation of caspase-1 resulted in a cytosolic accumulation of mitochondrial DNA in the absence of massive plasma membrane rupture. This indicates that GSDMD pores are not big enough to allow mitochondrial DNA to be released from the cell, but are big enough to induce its release from the mitochondrial matrix. This suggests a two-step mechanism for mitochondrial DNA release (and probably for the release of other mitochondrial DAMPs too) induced by GSDMs<sup>NT</sup> (53), with the first step being the accumulation of mitochondrial DNA in the cytosol and then its cellular release. Similarly, it has recently been shown that GSDMD<sup>NT</sup> induces NETosis formation in neutrophils, first helping to permeabilize the nuclear membrane and then allowing nuclear DNA release from the cell (15).

The inhibition of GSDMD<sup>NT</sup> plasma membrane permeabilization by punicalagin also inhibits mitochondrial network morphological alterations and mitochondrial DNA relocalisation into the cytosol despite the intracellular activation of caspase-1 and GSDMD processing. These data support the hypothesis that plasma membrane permeabilization might play an important role in mitochondrial collapse alongside MOMP and the mitochondrial localization of GSDMD<sup>NT</sup>. In addition, punicalagin blocks the release of pro-inflammatory cytokines such as IL-1 $\beta$  (19). In line with our findings, the recent development of drugs that block GSDM pore formation is an attractive strategy for controlling mitochondrial DNA release and other DAMPs and cytokines during regulated cell death and thus curbing the inflammatory response triggered by damaged tissue in many different diseases (54).

In conclusion, our study provides data on the mechanism involved in mitochondrial DNA release from the mitochondria matrix during pyroptosis and intrinsic apoptosis and in doing so highlights the role of GSDMs<sup>NT</sup> in permeabilizing the plasma membrane, which together with MOMP facilitates the efficient release of mitochondrial DNA.

## REFERENCES

1. Galluzzi, L., Vitale, I., Aaronson, S. A., Abrams, J. M., Adam, D., Agostinis, P., Alnemri, E. S., Altucci, L., Amelio, I., Andrews, D. W., Annicchiarico-Petruzzelli, M., Antonov, A. V., Arama, E., Baehrecke, E. H., Barlev, N. A., Bazan, N. G., Bernassola, F., Bertrand, M. J. M., Bianchi, K., Blagosklonny, M. V., Blomgren, K., Borner, C., Boya, P., Brenner, C., Campanella, M., Candi, E., Carmona-Gutierrez, D., Cecconi, F., Chan, F. K.-M., Chandel, N. S., Cheng, E. H., Chipuk, J. E., Cidlowski, J. A., Ciechanover, A., Cohen, G. M., Conrad, M., Cubillos-Ruiz, J. R., Czabotar, P. E., D'Angiolella, V., Dawson, T. M., Dawson, V. L., De Laurenzi, V., De Maria, R., Debatin, K.-M., DeBerardinis, R. J., Deshmukh, M., Di Daniele, N., Di Virgilio, F., Dixit, V. M., Dixon, S. J., Duckett, C. S., Dynlacht, B. D., El-Deiry, W. S., Elrod, J. W., Fimia, G. M., Fulda, S., García-Sáez, A. J., Garg, A. D., Garrido, C., Gavathiotis, E., Golstein, P., Gottlieb, E., Green, D. R., Greene, L. A., Gronemeyer, H., Gross, A., Hajnoczky, G., Hardwick, J. M., Harris, I. S., Hengartner, M. O., Hetz, C., Ichijo, H., Jäättelä, M., Joseph, B., Jost, P. J., Juin, P. P., Kaiser, W. J., Karin, M., Kaufmann, T., Kepp, O., Kimchi, A., Kitis, R. N., Klionsky, D. J., Knight, R. A., Kumar, S., Lee, S. W., Lemasters, J. J., Levine, B., Linkermann, A., Lipton, S. A., Lockshin, R. A., López-Otín, C., Lowe, S. W., Luedde, T., Lugli, E., MacFarlane, M., Madeo, F., Malewicz, M., Malorni, W., Manic, G., Marine, J.-C., Martin, S. J., Martinou, J.-C., Medema, J. P., Mehlen, P., Meier, P., Melino, S., Miao, E. A., Molkentin, J. D., Moll, U. M., Muñoz-Pinedo, C., Nagata, S., Nuñez, G., Oberst, A., Oren, M., Overholtzer, M., Pagano, M., Panaretakis, T., Pasparakis, M., Penninger, J. M., Pereira, D. M., Pervaiz, S., Peter, M. E., Piacentini, M., Pinton, P., Prehn, J. H. M., Puthalakath, H., Rabinovich, G. A., Rehm, M., Rizzuto, R., Rodrigues, C. M. P., Rubinsztein, D. C., Rudel, T., Ryan, K. M., Sayan, E., Scorrano, L., Shao, F., Shi, Y., Silke, J., Simon, H.-U., Sistigu, A., Stockwell, B. R., Strasser, A., Szabadkai, G., Tait, S. W. G., Tang, D., Tavernarakis, N., Thorburn, A., Tsujimoto, Y., Turk, B., Vanden Berghe, T., Vandenabeele, P., Vander Heiden, M. G., Villunger, A., Virgin, H. W., Vousden, K. H., Vucic, D., Wagner, E. F., Walczak, H., Wallach, D., Wang, Y., Wells, J. A., Wood, W., Yuan, J., Zakeri, Z., Zhivotovsky, B., Zitvogel, L., Melino, G., and Kroemer, G. (2018) Molecular mechanisms of cell death: recommendations of the Nomenclature

- Committee on Cell Death 2018. *Cell Death Differ.* **25**, 486–541
2. Broz, P., Pelegrín, P., and Shao, F. (2020) The gasdermins, a protein family executing cell death and inflammation. *Nat. Rev. Immunol.* **20**, 143–157
  3. Broz, P. and Dixit, V. M. (2016) Inflammasomes: mechanism of assembly, regulation and signalling. *Nat. Rev. Immunol.* **16**, 407–420
  4. Shi, J., Zhao, Y., Wang, K., Shi, X., Wang, Y., Huang, H., Zhuang, Y., Cai, T., Wang, F., and Shao, F. (2015) Cleavage of GSDMD by inflammatory caspases determines pyroptotic cell death. *Nature* **526**, 660–665
  5. Liu, X., Zhang, Z., Ruan, J., Pan, Y., Magupalli, V. G., Wu, H., and Lieberman, J. (2016) Inflammasome-activated gasdermin D causes pyroptosis by forming membrane pores. *Nature* **535**, 153–158
  6. Sborgi, L., Rühl, S., Mulvihill, E., Pipercevic, J., Heilig, R., Stahlberg, H., Farady, C. J., Müller, D. J., Broz, P., and Hiller, S. (2016) GSDMD membrane pore formation constitutes the mechanism of pyroptotic cell death. *EMBO J.* **35**, 1766–1778
  7. Wang, Y., Gao, W., Shi, X., Ding, J., Liu, W., He, H., Wang, K., and Shao, F. (2017) Chemotherapy drugs induce pyroptosis through caspase-3 cleavage of a gasdermin. *Nature* **547**, 99–103
  8. Rogers, C., Fernandes-Alnemri, T., Mayes, L., Alnemri, D., Cingolani, G., and Alnemri, E. S. (2017) Cleavage of DFNA5 by caspase-3 during apoptosis mediates progression to secondary necrotic/pyroptotic cell death. *Nat. Commun.* **8**, 14128
  9. Taabazuing, C. Y., Okondo, M. C., and Bachovchin, D. A. (2017) Pyroptosis and Apoptosis Pathways Engage in Bidirectional Crosstalk in Monocytes and Macrophages. *Cell Chem. Biol.* **24**, 507-514.e4
  10. Wei, M. C. (2001) Proapoptotic BAX and BAK: A Requisite Gateway to Mitochondrial Dysfunction and Death. *Science (80- )*. **292**, 727–730
  11. Li, P., Nijhawan, D., Budihardjo, I., Srinivasula, S. M., Ahmad, M., Alnemri, E. S., and Wang, X. (1997) Cytochrome c and dATP-Dependent Formation of Apaf-1/Caspase-9 Complex Initiates an Apoptotic Protease Cascade. *Cell* **91**, 479–489

12. Yu, J., Nagasu, H., Murakami, T., Hoang, H., Broderick, L., Hoffman, H. M., and Horng, T. (2014) Inflammasome activation leads to Caspase-1-dependent mitochondrial damage and block of mitophagy. *Proc. Natl. Acad. Sci.* **111**, 15514–15519
13. Tsuchiya, K., Nakajima, S., Hosojima, S., Thi Nguyen, D., Hattori, T., Manh Le, T., Hori, O., Mahib, M. R., Yamaguchi, Y., Miura, M., Kinoshita, T., Kushiyama, H., Sakurai, M., Shiroishi, T., and Suda, T. (2019) Caspase-1 initiates apoptosis in the absence of gasdermin D. *Nat. Commun.* **10**, 2091
14. Karmakar, M., Minns, M., Greenberg, E. N., Diaz-Aponte, J., Pestonjamas, K., Johnson, J. L., Rathkey, J. K., Abbott, D. W., Wang, K., Shao, F., Catz, S. D., Dubyak, G. R., and Pearlman, E. (2020) N-GSDMD trafficking to neutrophil organelles facilitates IL-1 $\beta$  release independently of plasma membrane pores and pyroptosis. *Nat. Commun.* **11**, 1–14
15. Chen, K. W., Monteleone, M., Boucher, D., Sollberger, G., Ramnath, D., Condon, N. D., von Pein, J. B., Broz, P., Sweet, M. J., and Schroder, K. (2018) Noncanonical inflammasome signaling elicits gasdermin D-dependent neutrophil extracellular traps. *Sci. Immunol.* **3**, eaar6676
16. Rogers, C., Erkes, D. A., Nardone, A., Aplin, A. E., Fernandes-Alnemri, T., and Alnemri, E. S. (2019) Gasdermin pores permeabilize mitochondria to augment caspase-3 activation during apoptosis and inflammasome activation. *Nat. Commun.* **10**, 1689
17. McArthur, K., Whitehead, L. W., Heddleston, J. M., Li, L., Padman, B. S., Oorschot, V., Geoghegan, N. D., Chappaz, S., Davidson, S., San Chin, H., Lane, R. M., Dramicanin, M., Saunders, T. L., Sugiana, C., Lessene, R., Osellame, L. D., Chew, T.-L., Dewson, G., Lazarou, M., Ramm, G., Lessene, G., Ryan, M. T., Rogers, K. L., van Delft, M. F., and Kile, B. T. (2018) BAK/BAX macropores facilitate mitochondrial herniation and mtDNA efflux during apoptosis. *Science (80-. )*. **359**, eaao6047
18. Riley, J. S., Quarato, G., Cloix, C., Lopez, J., O'Prey, J., Pearson, M., Chapman, J., Sesaki, H., Carlin, L. M., Passos, J. F., Wheeler, A. P., Oberst, A., Ryan, K. M., and Tait, S. W. (2018) Mitochondrial inner membrane permeabilisation enables mtDNA release during apoptosis. *EMBO J.* **37**, 1–16

19. Martin-Sanchez, F., Diamond, C., Zeitler, M., Gomez, A. I. A. I. A. I. A. I. A., Baroja-Mazo, A., Bagnall, J., Spiller, D., White, M., Daniels, M. M. J. D. M. J. D., Mortellaro, A., Penalver, M., Paszek, P., Steringer, J. P. J. P. J. P., Nickel, W., Brough, D., Pelegrin, P., Martín-Sánchez, F., Diamond, C., Zeitler, M., Gomez-Sánchez, A., Peñalver, M., Paszek, P., Steringer, J. P. J. P. J. P., Nickel, W., Brough, D., Pelegrín, P., Gomez, A. I. A. I. A. I. A. I. A., Baroja-Mazo, A., Bagnall, J., Spiller, D., White, M., Daniels, M. M. J. D. M. J. D., Mortellaro, A., Peñalver, M., Paszek, P., Steringer, J. P. J. P. J. P., Nickel, W., Brough, D., Pelegrín, P., Pelegrin, P., Martín-Sánchez, F., Diamond, C., Zeitler, M., Gomez, A. I. A. I. A. I. A. I. A., Baroja-Mazo, A., Bagnall, J., Spiller, D., White, M., Daniels, M. M. J. D. M. J. D., Mortellaro, A., Peñalver, M., Paszek, P., Steringer, J. P. J. P. J. P., Nickel, W., Brough, D., Pelegrín, P., Gomez-Sánchez, A., Peñalver, M., Paszek, P., Steringer, J. P. J. P. J. P., Nickel, W., Brough, D., Pelegrín, P., Gomez, A. I. A. I. A. I. A. I. A., Baroja-Mazo, A., Bagnall, J., Spiller, D., White, M., Daniels, M. M. J. D. M. J. D., Mortellaro, A., Peñalver, M., Paszek, P., Steringer, J. P. J. P. J. P., Nickel, W., Brough, D., and Pelegrin, P. (2016) Inflammasome-dependent IL-1 $\beta$  release depends upon membrane permeabilisation. *Cell Death Differ.* **23**, 1219–1231
20. Loomis, W. P., den Hartigh, A. B., Cookson, B. T., and Fink, S. L. (2019) Diverse small molecules prevent macrophage lysis during pyroptosis. *Cell Death Dis.* **10**, 326
21. Solle, M., Labasi, J., Perregaux, D. G., Stam, E., Petrushova, N., Koller, B. H., Griffiths, R. J., and Gabel, C. A. (2000) Altered Cytokine Production in Mice Lacking P2X7 Receptors. *J. Biol. Chem.* **276**, 125–132
22. Mayor, A., Tardivel, A., Martinon, F., Pe, V., Pétrilli, V., Mayor, A., Tardivel, A., and Tschopp, J. (2006) Gout-associated uric acid crystals activate the NALP3 inflammasome. *Nature* **440**, 237–241
23. Kuida, K., Lippke, J., Ku, G., Harding, M., Livingston, D., Su, M., and Flavell, R. (1995) Altered cytokine export and apoptosis in mice deficient in interleukin-1 beta converting enzyme. *Science (80- )*. **267**, 2000–2003
24. Barberà-Cremades, M., Baroja-Mazo, A., Gomez, A. I. A. I., Machado, F., Di Virgilio, F., Pelegrín, P., Barberà-Cremades, M., Baroja-Mazo, A., Gomez, A. I. A. I., Machado, F., Di

- Virgilio, F., and Pelegrin, P. (2012) P2X7 receptor-stimulation causes fever via PGE2 and IL-1 $\beta$  release. *FASEB J.* **26**, 2951–2962
25. Wieckowski, M. R., Giorgi, C., Lebedzinska, M., Duszynski, J., and Pinton, P. (2009) Isolation of mitochondria-associated membranes and mitochondria from animal tissues and cells. *Nat. Protoc.* **4**, 1582–1590
26. de Torre-Minguela, C., Barberà-Cremades, M., Gómez, A. I., Martín-Sánchez, F., and Pelegrín, P. (2016) Macrophage activation and polarization modify P2X7 receptor secretome influencing the inflammatory process. *Sci. Rep.* **6**, 22586
27. Wojtala, A., Bonora, M., Malinska, D., Pinton, P., Duszynski, J., and Wieckowski, M. R. (2014) Methods to Monitor ROS Production by Fluorescence Microscopy and Fluorometry. In *Methods in Enzymology* pp. 243–262,
28. Russo, H. M., Rathkey, J., Boyd-Tressler, A., Katsnelson, M. A., Abbott, D. W., and Dubyak, G. R. (2016) Active Caspase-1 Induces Plasma Membrane Pores That Precede Pyroptotic Lysis and Are Blocked by Lanthanides. *J. Immunol.* **197**, 1353–1367
29. Evavold, C. L., Ruan, J., Tan, Y., Xia, S., Wu, H., and Kagan, J. C. (2018) The pore-forming protein gasdermin D regulates interleukin-1 secretion from living macrophages. *Immunity* **48**, 35-44.e6
30. de Vasconcelos, N. M., Van Opdenbosch, N., Van Gorp, H., Parthoens, E., and Lamkanfi, M. (2018) Single-cell analysis of pyroptosis dynamics reveals conserved GSDMD-mediated subcellular events that precede plasma membrane rupture. *Cell Death Differ.* **1**
31. Andreyev, A. Y., Kushnareva, Y. E., and Starkov, A. A. (2005) Mitochondrial metabolism of reactive oxygen species. *Biochem.* **70**, 246–264
32. Bauernfeind, F. G., Horvath, G., Stutz, A., Alnemri, E. S., MacDonald, K., Speert, D., Fernandes-Alnemri, T., Wu, J., Monks, B. G., Fitzgerald, K. A., Hornung, V., and Latz, E. (2009) Cutting Edge: NF- $\kappa$ B Activating Pattern Recognition and Cytokine Receptors License NLRP3 Inflammasome Activation by Regulating NLRP3 Expression. *J. Immunol.* **183**, 787–791
33. Cai, J. and Jones, D. P. (1998) Superoxide in apoptosis. Mitochondrial generation triggered

- by cytochrome c loss. *J. Biol. Chem.* **273**, 11401–11404
34. Robinson, K. M., Janes, M. S., Pehar, M., Monette, J. S., Ross, M. F., Hagen, T. M., Murphy, M. P., and Beckman, J. S. (2006) Selective fluorescent imaging of superoxide in vivo using ethidium-based probes. *Proc. Natl. Acad. Sci.* **103**, 15038–15043
  35. Zielonka, J. and Kalyanaraman, B. (2010) Hydroethidine- and MitoSOX-derived red fluorescence is not a reliable indicator of intracellular superoxide formation: Another inconvenient truth. *Free Radic. Biol. Med.* **48**, 983–1001
  36. Polster, B. M., Nicholls, D. G., Ge, S. X., and Roelofs, B. A. (2014) Use of Potentiometric Fluorophores in the Measurement of Mitochondrial Reactive Oxygen Species. In *Methods in Enzymology* pp. 225–250,
  37. Imao, T. and Nagata, S. (2013) Apaf-1- and Caspase-8-independent apoptosis. *Cell Death Differ.* **20**, 343–352
  38. Chauhan, D., Bartok, E., Gaidt, M. M., Bock, F. J., Herrmann, J., Seeger, J. M., Broz, P., Beckmann, R., Kashkar, H., Tait, S. W. G., Müller, R., and Hornung, V. (2018) BAX/BAK-Induced Apoptosis Results in Caspase-8-Dependent IL-1 $\beta$  Maturation in Macrophages. *Cell Rep.* **25**, 2354-2368.e5
  39. Martín-Sánchez, F., Martínez-García, J. J., Muñoz-García, M., Martínez-Villanueva, M., Noguera-Velasco, J. A., Andreu, D., Rivas, L., and Pelegrín, P. (2017) Lytic cell death induced by melittin bypasses pyroptosis but induces NLRP3 inflammasome activation and IL-1 $\beta$  release. *Cell Death Dis.* **8**, e2984–e2984
  40. Kuznetsov, A. V., Veksler, V., Gellerich, F. N., Saks, V., Margreiter, R., and Kunz, W. S. (2008) Analysis of mitochondrial function in situ in permeabilized muscle fibers, tissues and cells. *Nat. Protoc.* **3**, 965–976
  41. Altschuld, R. A., Wenger, W. C., Lamka, K. G., Kindig, O. R., Capen, C. C., Mizuhira, V., Vander Heide, R. S., and Brierley, G. P. (1985) Structural and functional properties of adult rat heart myocytes lysed with digitonin. *J. Biol. Chem.* **260**, 14325–14334
  42. Zhang, Q., Raoof, M., Chen, Y., Sumi, Y., Sursal, T., Junger, W., Brohi, K., Itagaki, K., Hauser, C. J., Yang, H., Yang, H., Wang, H., Wang, H., Ju, Z., Ju, Z., Ragab, A. A., Ragab, A. A.,

- Lundback, P., Lundback, P., Long, W., Long, W., Valdes-Ferrer, S. I., Valdes-Ferrer, S. I., He, M., He, M., Pribis, J. P., Pribis, J. P., Li, J., Lu, B., Lu, B., Gero, D., Gero, D., Szabó, C., Szabó, C., Antoine, D. J., Antoine, D. J., Harris, H. E., Harris, H. E., Golenbock, D. T., Golenbock, D. T., Meng, J., Meng, J., Roth, J., Roth, J., Chavan, S. S., Chavan, S. S., Andersson, U., Andersson, U., Billiar, T. R., Billiar, T. R., Tracey, K. J., Tracey, K. J., Al-Abed, Y., and Al-Abed, Y. (2010) Circulating mitochondrial DAMPs cause inflammatory responses to injury. *J. Exp. Med.* **464**, 104–107
43. Itagaki, K., Kaczmarek, E., Lee, Y. T., Tang, I. T., Isal, B., Adibnia, Y., Sandler, N., Grimm, M. J., Segal, B. H., Otterbein, L. E., and Hauser, C. J. (2015) Mitochondrial DNA Released by Trauma Induces Neutrophil Extracellular Traps. *PLoS One* **10**, e0120549
44. Huang, L. S., Hong, Z., Wu, W., Xiong, S., Zhong, M., Gao, X., Rehman, J., and Malik, A. B. (2020) mtDNA Activates cGAS Signaling and Suppresses the YAP-Mediated Endothelial Cell Proliferation Program to Promote Inflammatory Injury. *Immunity* **52**, 475-486.e5
45. Hajizadeh, S., DeGroot, J., TeKoppele, J. M., Tarkowski, A., and Collins, L. V. (2003) Extracellular mitochondrial DNA and oxidatively damaged DNA in synovial fluid of patients with rheumatoid arthritis. *Arthritis Res. Ther.* **5**, R234–R240
46. Bae, J. H., Jo, S. I., Kim, S. J., Lee, J. M., Jeong, J. H., Kang, J. S., Cho, N.-J., Kim, S. S., Lee, E. Y., and Moon, J.-S. (2019) Circulating Cell-Free mtDNA Contributes to AIM2 Inflammasome-Mediated Chronic Inflammation in Patients with Type 2 Diabetes. *Cells* **8**, 328
47. Oka, T., Hikoso, S., Yamaguchi, O., Taneike, M., Takeda, T., Tamai, T., Oyabu, J., Murakawa, T., Nakayama, H., Nishida, K., Akira, S., Yamamoto, A., Komuro, I., and Otsu, K. (2012) Mitochondrial DNA that escapes from autophagy causes inflammation and heart failure. *Nature* **485**, 251–255
48. Kim, J., Gupta, R., Blanco, L. P., Yang, S., Shteinifer-Kuzmine, A., Wang, K., Zhu, J., Yoon, H. E., Wang, X., Kerkhofs, M., Kang, H., Brown, A. L., Park, S.-J., Xu, X., Zandee van Rilland, E., Kim, M. K., Cohen, J. I., Kaplan, M. J., Shoshan-Barmatz, V., and Chung, J. H. (2019) VDAC oligomers form mitochondrial pores to release mtDNA fragments and promote lupus-like disease. *Science (80-. ).* **366**, 1531–1536

49. White, M. J., McArthur, K., Metcalf, D., Lane, R. M., Cambier, J. C., Herold, M. J., van Delft, M. F., Bedoui, S., Lessene, G., Ritchie, M. E., Huang, D. C. S., and Kile, B. T. (2014) Apoptotic Caspases Suppress mtDNA-Induced STING-Mediated Type I IFN Production. *Cell* **159**, 1549–1562
50. Rongvaux, A., Jackson, R., Harman, C. C. D., Li, T., West, A. P., de Zoete, M. R., Wu, Y., Yordy, B., Lakhani, S. A., Kuan, C.-Y., Taniguchi, T., Shadel, G. S., Chen, Z. J., Iwasaki, A., and Flavell, R. A. (2014) Apoptotic Caspases Prevent the Induction of Type I Interferons by Mitochondrial DNA. *Cell* **159**, 1563–1577
51. Banerjee, I., Behl, B., Mendonca, M., Shrivastava, G., Russo, A. J., Menoret, A., Ghosh, A., Vella, A. T., Vanaja, S. K., Sarkar, S. N., Fitzgerald, K. A., and Rathinam, V. A. K. (2018) Gasdermin D Restrains Type I Interferon Response to Cytosolic DNA by Disrupting Ionic Homeostasis. *Immunity* 1–14
52. Nerlich, A., Mieth, M., Letsiou, E., Fatykhova, D., Zscheppang, K., Imai-Matsushima, A., Meyer, T. F., Paasch, L., Mitchell, T. J., Tönnies, M., Bauer, T. T., Schneider, P., Neudecker, J., Rückert, J. C., Eggeling, S., Schimek, M., Witzernath, M., Suttorp, N., Hippenstiel, S., and Hocke, A. C. (2018) Pneumolysin induced mitochondrial dysfunction leads to release of mitochondrial DNA. *Sci. Rep.* **8**, 182
53. Grazioli, S. and Pugin, J. (2018) Mitochondrial Damage-Associated Molecular Patterns: From Inflammatory Signaling to Human Diseases. *Front. Immunol.* **9**
54. Hu, J. J., Liu, X., Xia, S., Zhang, Z., Zhang, Y., Zhao, J., Ruan, J., Luo, X., Lou, X., Bai, Y., Wang, J., Hollingsworth, L. R., Magupalli, V. G., Zhao, L., Luo, H. R., Kim, J., Lieberman, J., and Wu, H. (2020) FDA-approved disulfiram inhibits pyroptosis by blocking gasdermin D pore formation. *Nat. Immunol.* **21**, 736–745

**Acknowledgements:** We thank F. Shao (National Institute of Biological Sciences, Beijing, China) for kindly supplying GSDMD and GSDME expression plasmids, L Rivas (CSIC, Madrid, Spain) for kindly supplying melittin and M.C. Baños (IMIB-Arrixaca, Murcia, Spain) for technical assistance.

**Funding:** This work was supported by grants from *FEDER/Ministerio de Ciencia, Innovación y Universidades – Agencia Estatal de Investigación* (grant SAF2017-88276-R), *Fundación Séneca* (grants 20859/PI/18, 21081/PDC/19 and 0003/COVI/20) and the European Research Council (grants ERC-2013-CoG 614578 and ERC-2019-PoC grant 899636).

**Author contributions:** CdT-M and PP conceived and designed the experiments. CdT-M and AIG performed the experiments. CdT-M analyzed the data. IC bred and provided the knock-out mice and bone-marrow samples. CdT-M and PP prepared the figures and wrote the paper.

**Competing interests:** The authors declare that they have no competing interests.

**Data and materials availability:** All data and materials are available from the authors upon reasonable request.

## FIGURE LEGENDS

### Figure 1. NLRP3 inflammasome activation induces GSDMD-dependent mitochondrial network fragmentation

- A, B Different genotypes from mouse macrophages (as indicated) were primed for 4 h with LPS (10 ng/ml) and then stimulated for 20 min with ATP (3 mM), nigericin (5  $\mu$ M) or with antimycin A (10  $\mu$ M). Whole cell lysates (A), or cytosolic and organelle fractions (B) were analyzed by immunoblot for the proteins indicated.
- C Deconvolved maximum intensity projections of z-stack images of macrophages primed for 4 h with LPS (10 ng/ml) and then stimulated for 10 min with nigericin (5  $\mu$ M) and stained with TOMM20 antibodies (green) and DAPI (blue). Scale bar represents 8  $\mu$ m.

Data information: All immunoblots and microscopy images are representative of three independent experiments.

### Figure 2. GSDMD induces mitochondrial DNA release after NLRP3 inflammasome activation

- A Kinetic of MitoSOX fluorescence from macrophages with different genotypes (as indicated) primed for 4 h with LPS (10 ng/ml). Then fluorescence was monitored for 50 min while stimulating with ATP (3 mM), nigericin (5  $\mu$ M) or antimycin A (10  $\mu$ M).
- B Quantification of mitochondrial DNA presence in the cytosolic fraction from macrophages with different genotypes (as indicated) primed as in A and stimulated for 20 min with nigericin (10 $\mu$ M).
- C Deconvolved maximum intensity projections of z-stack images of macrophages primed as in A and stimulated or not for 10 min with nigericin (5  $\mu$ M) and then stained with anti-DNA antibodies (red), TOMM20 antibodies (green) and DAPI (blue). Scale bar represents 5  $\mu$ m.
- D Quantification of mitochondrial DNA release in supernatant (SPN) from macrophages with different genotypes (as indicated) primed as in A and stimulated for 20 min with nigericin (10  $\mu$ M).

Data information: Data in A are means  $\pm$  SEM of three independent experiments and were normalized with 100% considered the average fluorescence of antimycin A at 45 min. Data in B and D are means  $\pm$  SEM of four-five independent experiments. Statistical analyses were performed using non-parametric Mann–Whitney t-tests. Data were considered significant when \*  $P < 0.05$ . Microscopy images of panel C are representative of three independent experiments.

**Figure 3. Pysin inflammasome activation and GSDMD<sup>NT</sup> induce mitochondrial DNA release**

- A Macrophages with different genotypes (as indicated) were primed for 4 h with LPS (10 ng/ml) and then stimulated at indicated times with nigericin (5  $\mu$ M) or with the toxin B from *Clostridium difficile* (TcdB) (1  $\mu$ g/ml). Cell extracts were analyzed using immunoblot for the proteins indicated.
- B IL-1 $\beta$  and LDH release detected in cell-free supernatants from *Nlrp3*<sup>-/-</sup> macrophages primed and stimulated with TcdB as indicated in A.
- C Deconvolved maximum intensity projections of z-stack images of *Nlrp3*<sup>-/-</sup> and *Casp1/11*<sup>-/-</sup> macrophages primed and stimulated with TcdB as indicated in A and stained with TOMM20 antibodies (green) and DAPI (blue). Scale bar represents 8  $\mu$ m.
- D Mitochondrial DNA release detected in cell-free supernatants from *Nlrp3*<sup>-/-</sup> macrophages primed and stimulated with TcdB as indicated in A.
- E Deconvolved maximum intensity projections of z-stack images of HEK293T after 16 h transfected with plasmids encoding for human full-length GSDMD or GSDMD<sup>NT</sup> (1-275) and stained with TOMM20 antibodies (green) and DAPI (blue). Scale bar represents 10  $\mu$ m.
- F Quantification of HMGB1 and mitochondrial DNA released in cell free supernatant obtained from HEK293T transfected as in E.

Data information: Data in panels B, D and F are means  $\pm$  SEM from four-five independent experiments. Statistical analyses were performed using non-parametric Mann–Whitney t-tests. Data were considered significant when \* $P < 0.05$ , \*\* $P < 0.01$ . Immunoblots in panel A and microscopy images of panels C and E are representative of three independent experiments.

**Figure 4. Mitochondrial DNA release is also promoted by GSDME**

- A Wild type macrophages were primed for 4 h with LPS (10 ng/ml) and then stimulated with nigericin (10 $\mu$ M), *Casp1/11*<sup>-/-</sup> macrophages were treated with DMSO or staurosporin (1  $\mu$ M) during the indicated times. Cell lysates were analyzed by immunoblot for the indicated proteins.
- B Macrophages of different genotypes (as indicated) were primed and stimulated as in A. LDH and HMGB1 release was determined in cell-free supernatant.
- C Deconvolved maximum intensity projections of z-stack images of *Casp1/11*<sup>-/-</sup> macrophages treated for 4 h with DMSO or staurosporin (1  $\mu$ M) and stained with TOMM20 antibodies (green) and DAPI (blue). Scale bar represents 10  $\mu$ m.
- D Quantification of mitochondrial DNA released in cell free supernatant obtained from macrophages stimulated as in A.
- E Quantification of HMGB1 released in cell free supernatant obtained from HEK293T expressing human GSDME<sup>NT</sup> (1-270) for 16 h.
- F Deconvolved maximum intensity projection of z-stack image of HEK293T expressing human GSDME<sup>NT</sup> as in E and stained with TOMM20 antibodies (green) and DAPI (blue). Scale bar represents 10  $\mu$ m.
- G Quantification of mitochondrial DNA released in cell free supernatant obtained from expressing human GSDME<sup>NT</sup> as in E.

Data information: Immunoblots in panel A and microscopic images in panels C and F are representative of three independent experiments. For panels B, D, E and G, data are means  $\pm$  SEM from at least four independent experiments. Statistical analyses were performed using non-parametric Mann–Whitney t-tests. Data were considered significant when \*P < 0.05, \*\*P < 0.01, or \*\*\*P < 0.001.

**Figure 5. GSDMD promotes mitochondrial DNA relocalisation to the cytosol in the absence of cell lysis**

- A Kinetic of YoPro-1 uptake and MitoSOX fluorescence in wild type macrophages primed for 4 h with LPS (10 ng/ml) and then stimulated with nigericin (5  $\mu$ M, as shown by the arrow) in the presence or not of glycine (5 mM). Glycine was added 15 min before and during stimulation.
- B IL-1 $\beta$  and LDH was determined in cell-free supernatant of macrophages stimulated as in A but after 20 or 40 min of nigericin as indicated.
- C Cytosolic and organelle fraction of macrophages stimulated as in B were analyzed by immunoblot for the indicated proteins.
- D Deconvolved maximum intensity projections of z-stack images of wild type macrophages primed with LPS as in A and then stimulated for 20 or 40 min with nigericin (5  $\mu$ M) in presence or not of glycine (5 mM), and stained with TOMM20 antibodies (green) and DAPI (blue). Scale bar represents 10  $\mu$ m.
- E Quantification of mitochondrial DNA in supernatants and cytosol of macrophages primed and stimulated as in B.

Data information: Data in panel A are means  $\pm$  SEM from three independent experiments. Data in panels B and E are means  $\pm$  SEM from three-six independent experiments. Statistical analyses were performed using non-parametric Mann–Whitney t-tests. Data were considered significant when \*P < 0.05, \*\*P < 0.01. Immunoblots of panel C and microscopy images of panel D are representative of three independent experiments.

**Figure 6. GSDMD<sup>NT</sup> plasma membrane pore activity is required for mitochondrial damage**

- A Wild type macrophages were primed for 4 h with LPS (10 ng/ml) and then stimulated for 20 min with nigericin (5  $\mu$ M) in the presence or not of punicalagin (50  $\mu$ M). Punicalagin was added 10 min before and during nigericin stimulation. Cell lysates were analyzed by immunoblot for the indicated proteins.

- B Kinetic of YoPro-1 uptake in macrophages primed and stimulated as in A. Nigericin was added as shown by the arrow.
- C LDH and mitochondrial DNA presence in cell-free supernatants from macrophages primed and stimulated as in A.
- D Deconvolved maximum intensity projections of z-stack images of wild type macrophages primed and stimulated as in A, but using 25  $\mu$ M of punicalagin. In the images indicated, nigericin and punicalagin were removed from the cell culture after 15 min of stimulation and cells were fixed after 10 min washout. Cells were stained with DNA antibodies (red), TOMM20 antibodies (green) and DAPI (blue). Scale bar represents 10  $\mu$ m.
- E Kinetic of MitoSOX fluorescence in macrophages primed and stimulated as in A. Nigericin was added as shown by the arrow.

Data information: Immunoblots in panel A and microscopy images in panel D are representative of three independent experiments. Data in panels B and E are means  $\pm$  SEM from three independent experiments. Data in panel C represent means  $\pm$  SEM from three-five independent experiments. Statistical analyses were performed using non-parametric Mann–Whitney t-tests. Data were considered significant when \*P < 0.05, \*\*P < 0.01

# Figure 1

# Figure 1

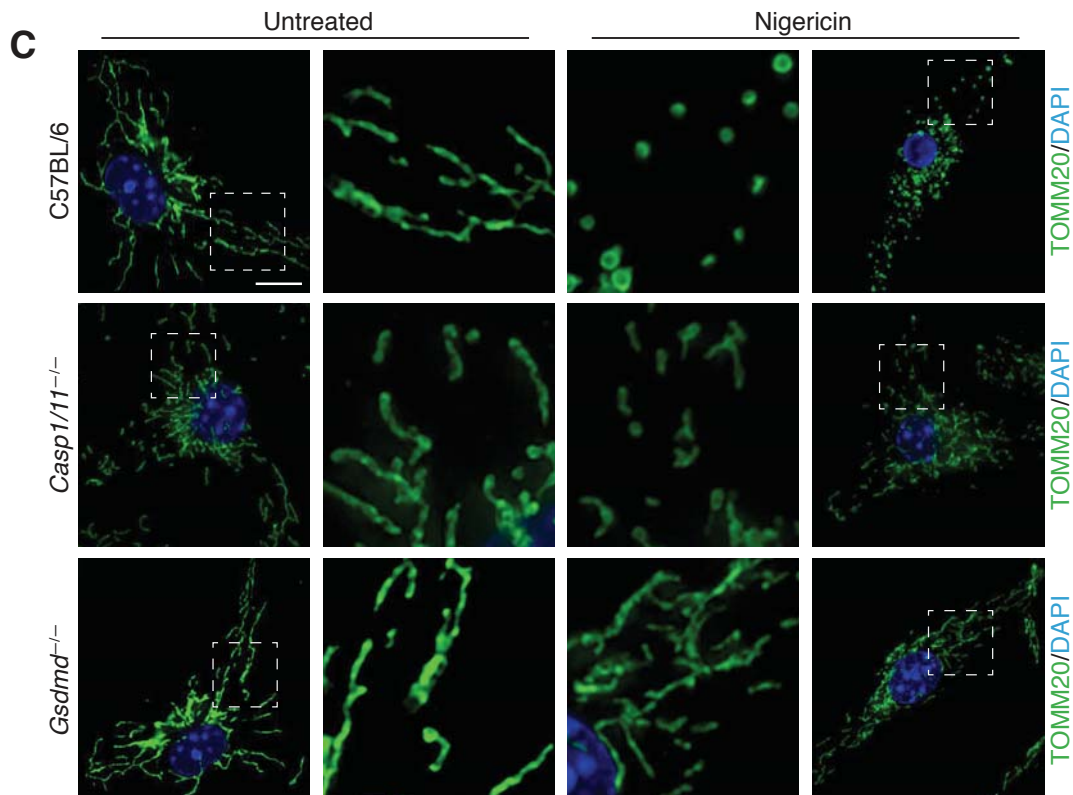
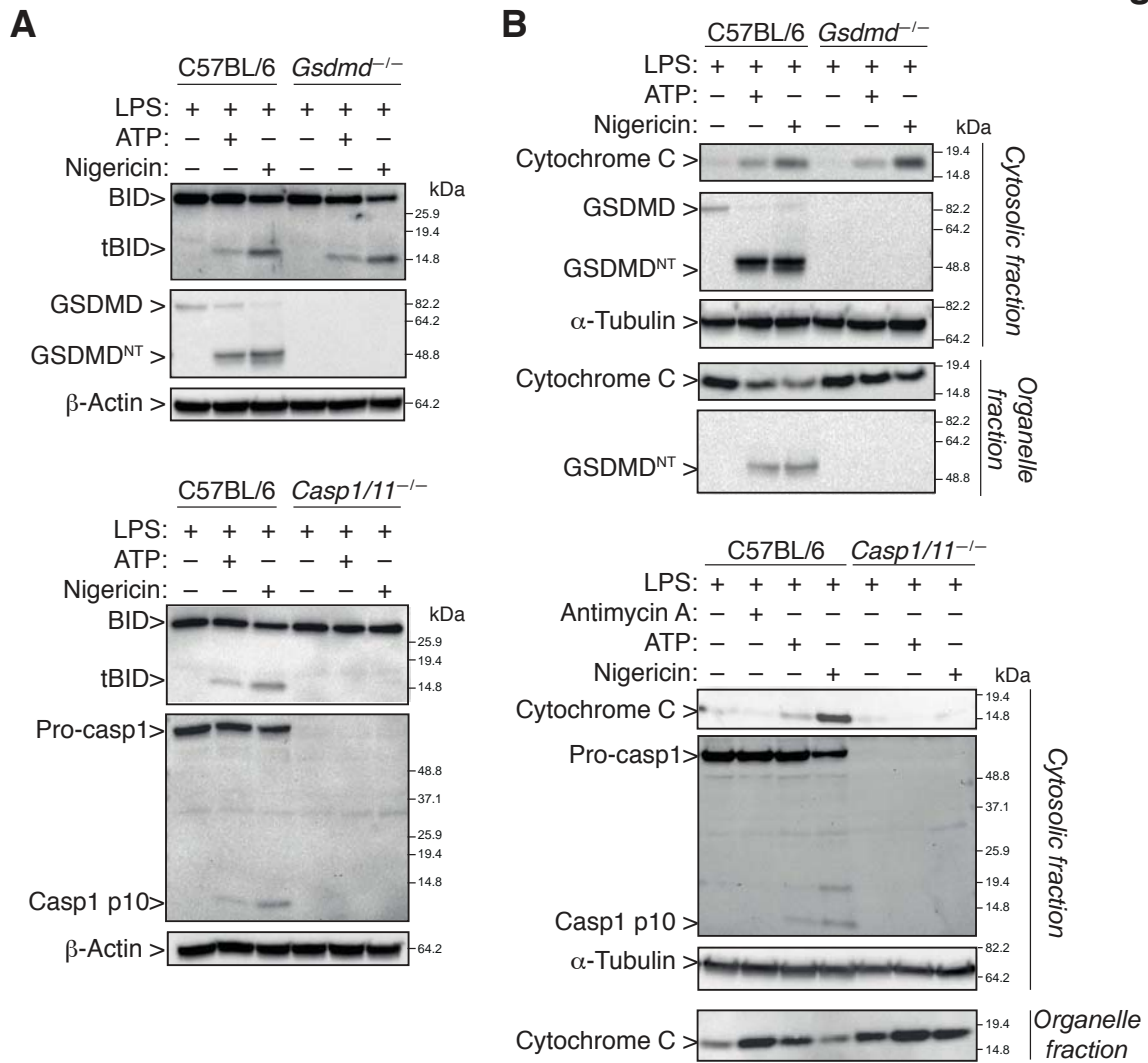


# Figure 2

# Figure 2

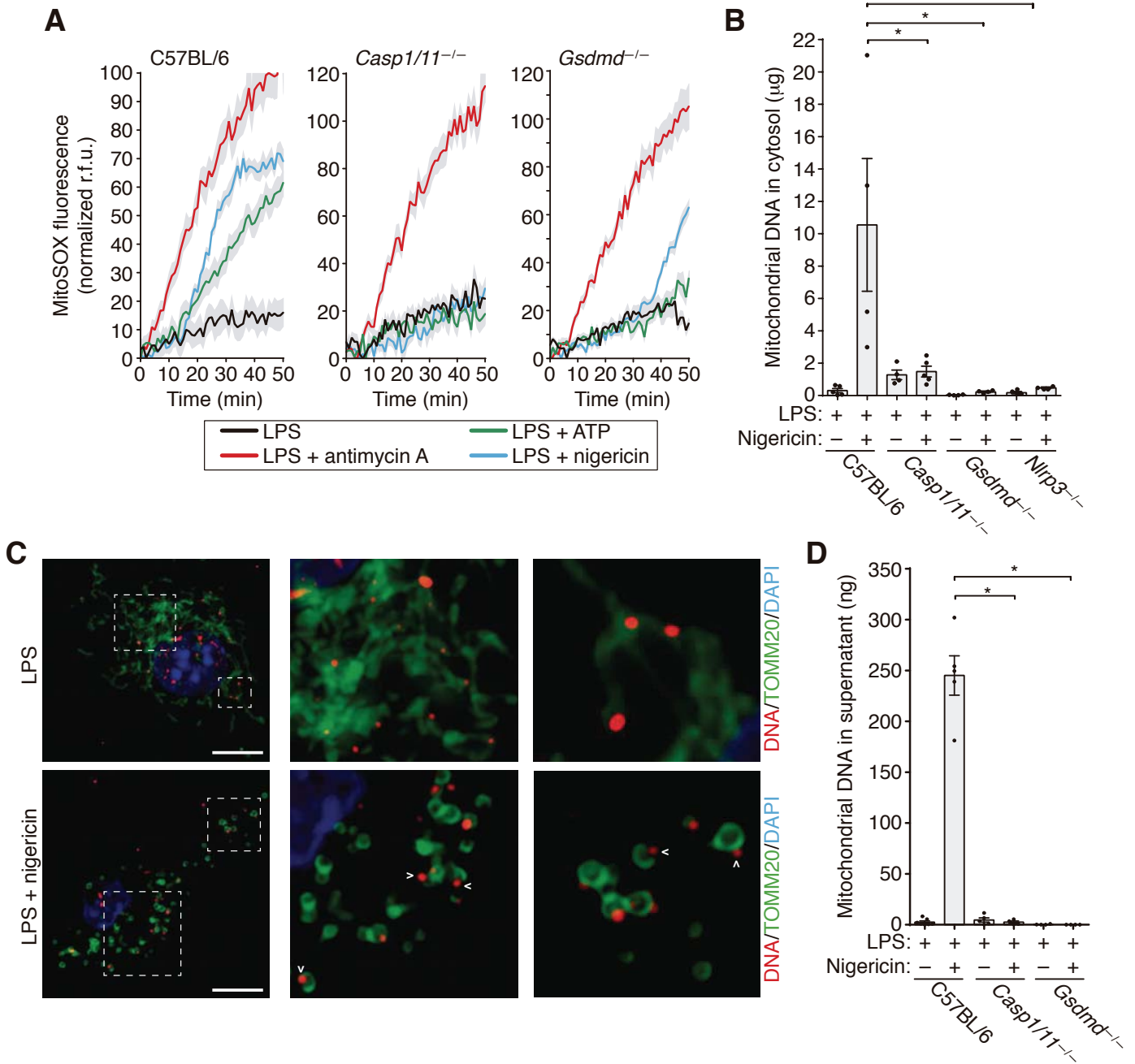


# Figure 3

# Figure 3

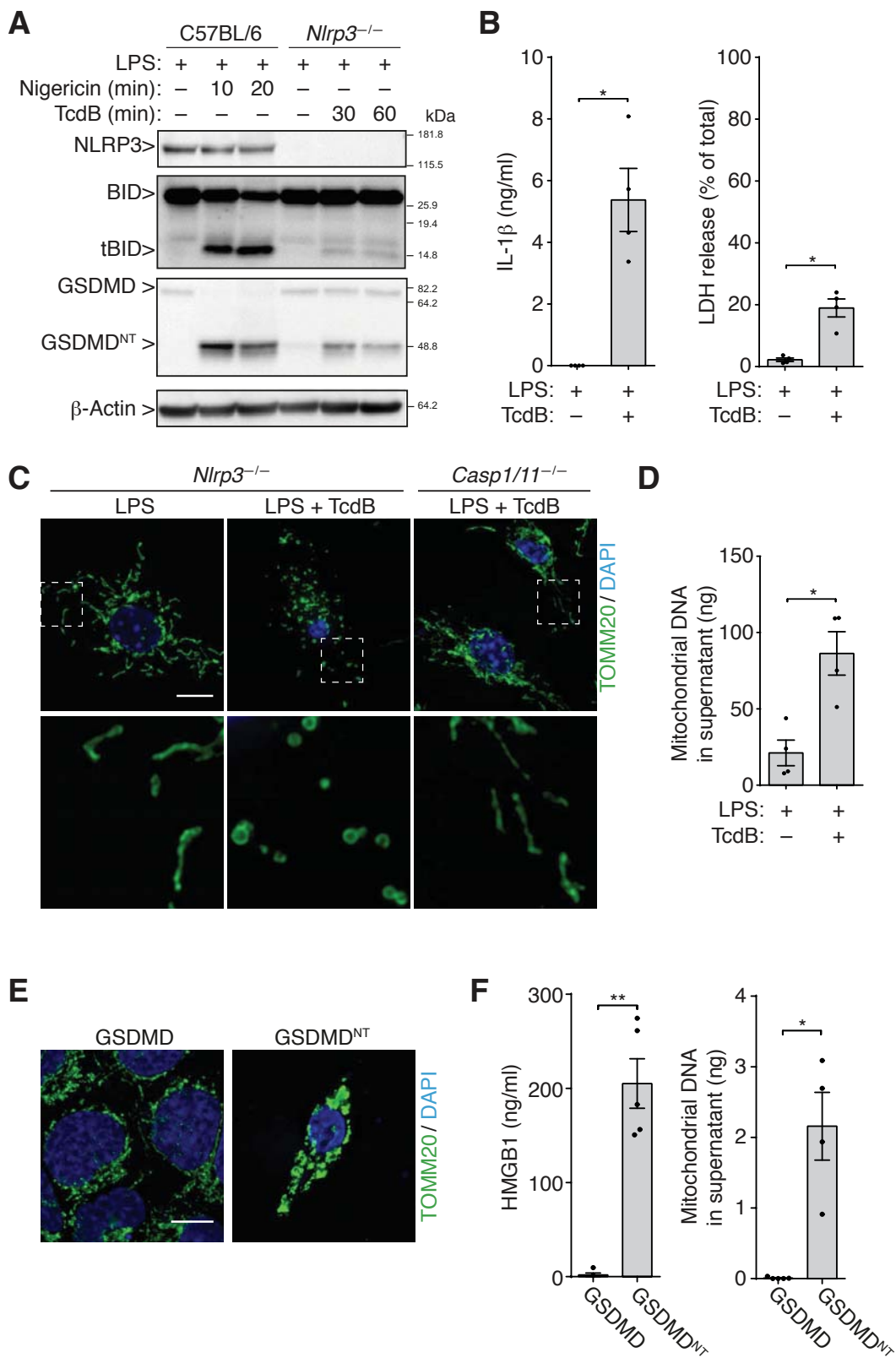


# Figure 4

# Figure 4

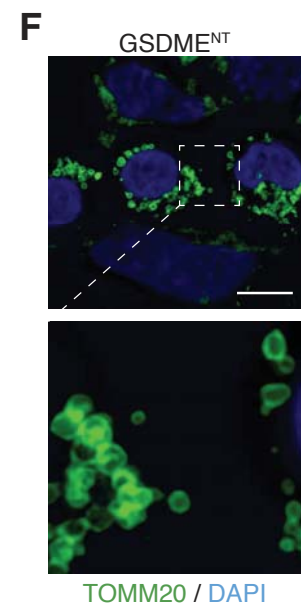
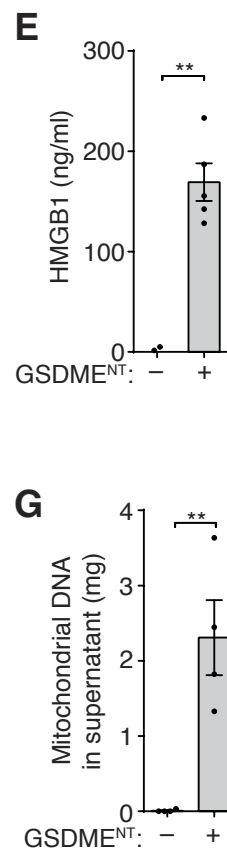
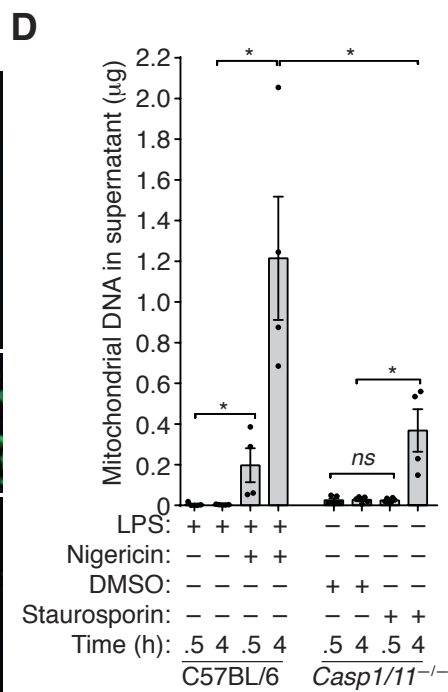
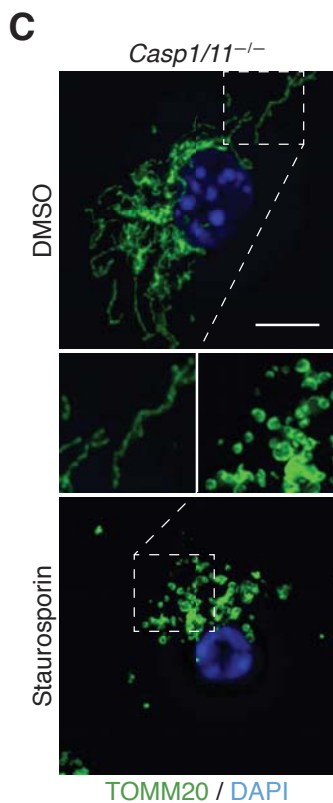
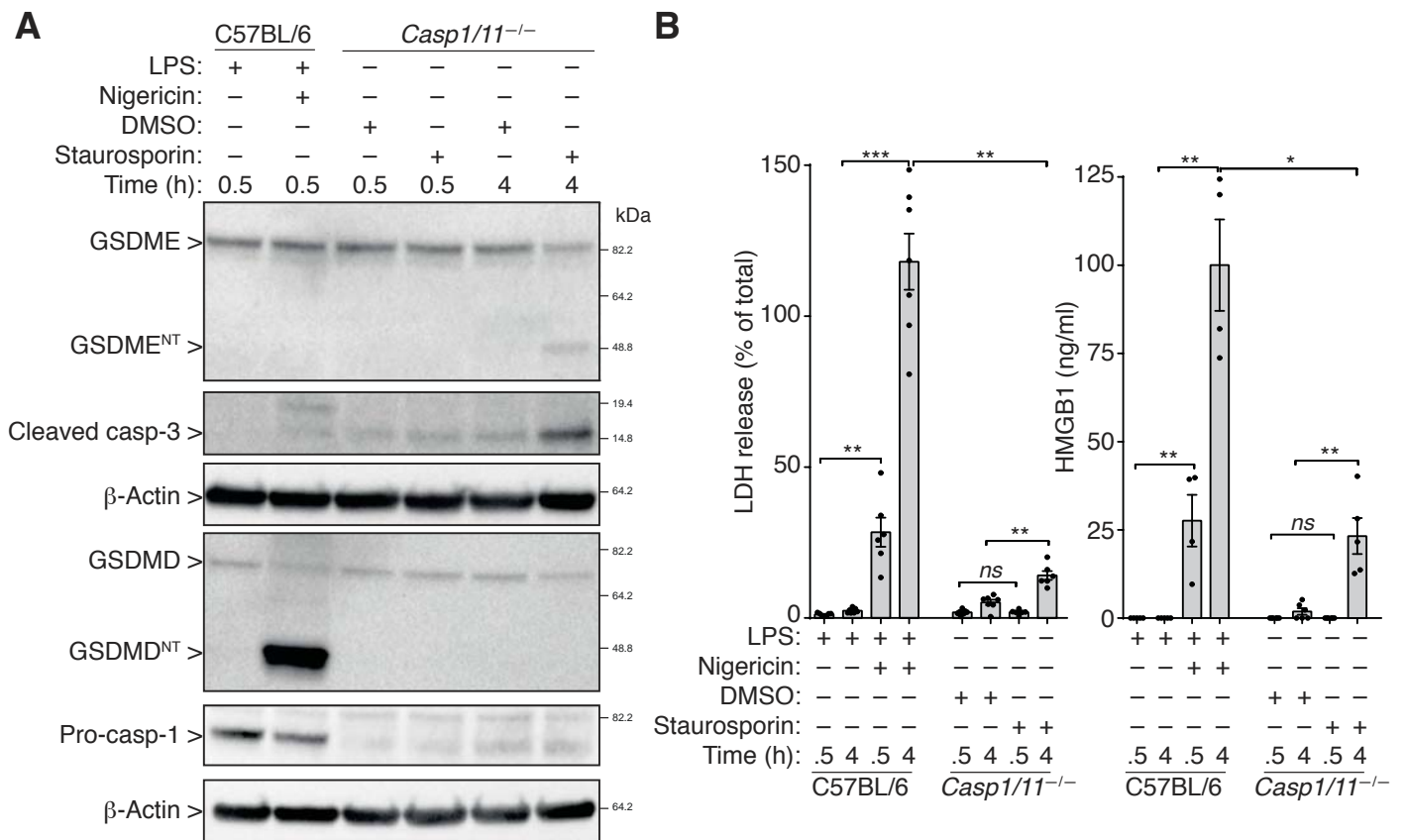


# Figure 5

# Figure 5

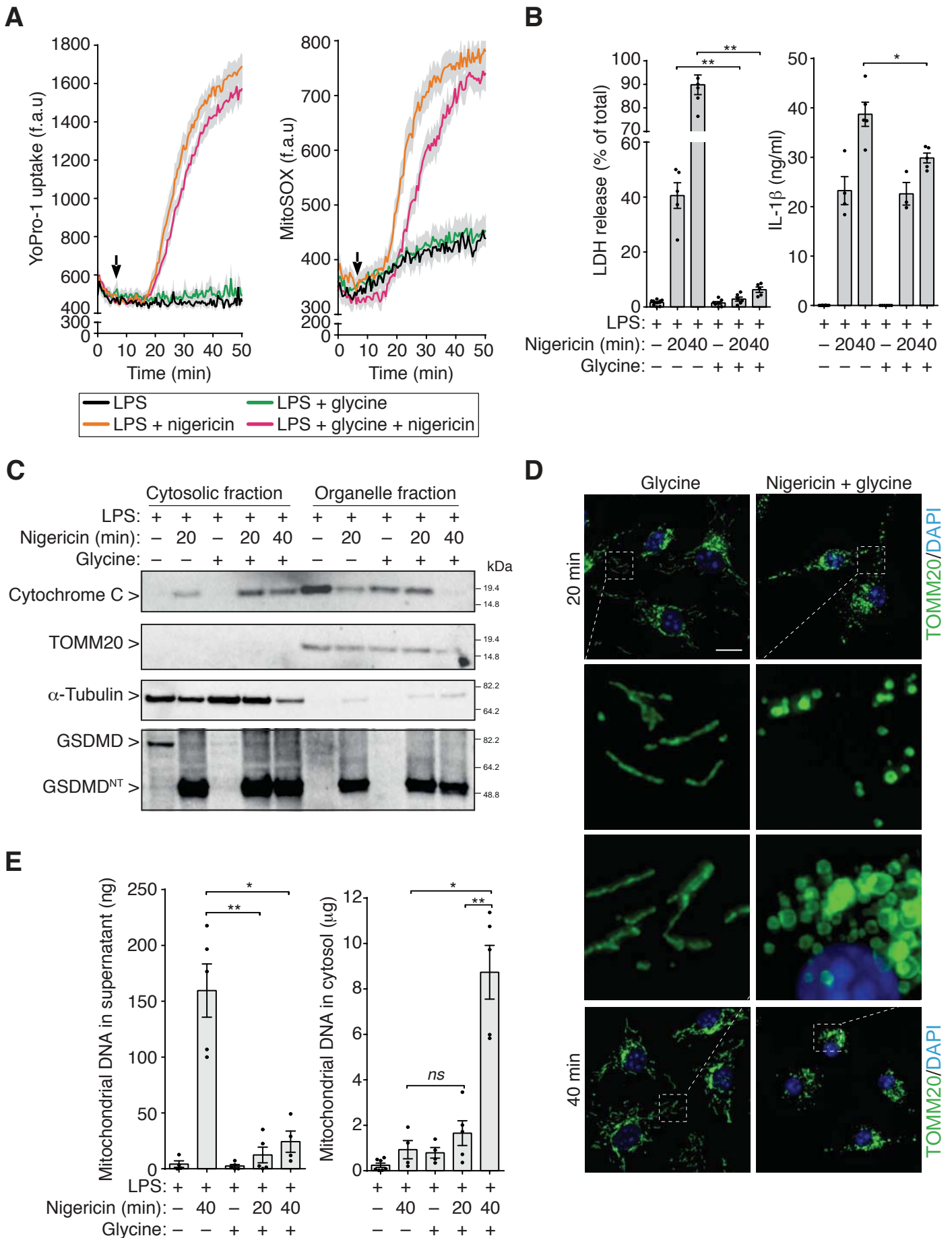
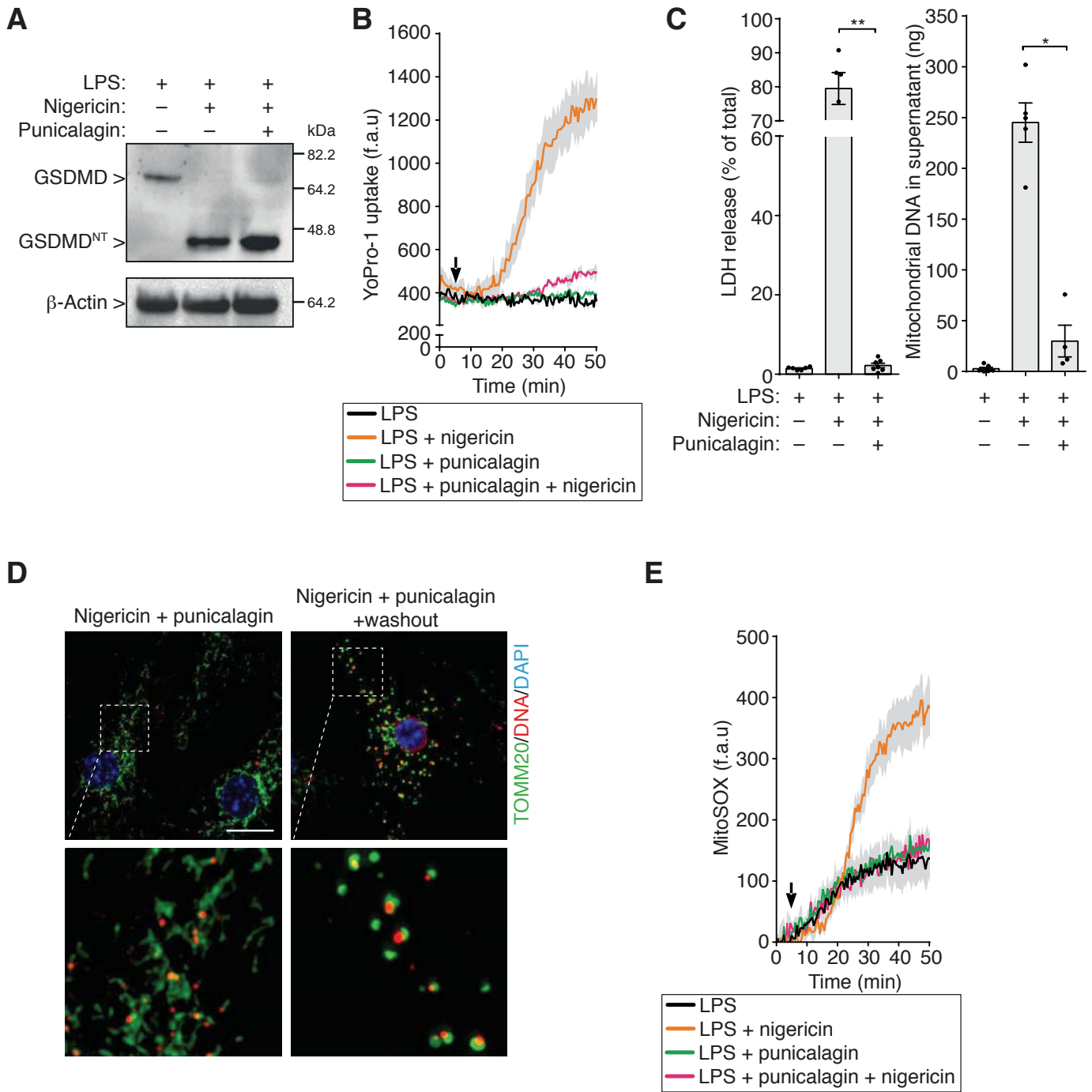


# Figure 6

# Figure 6

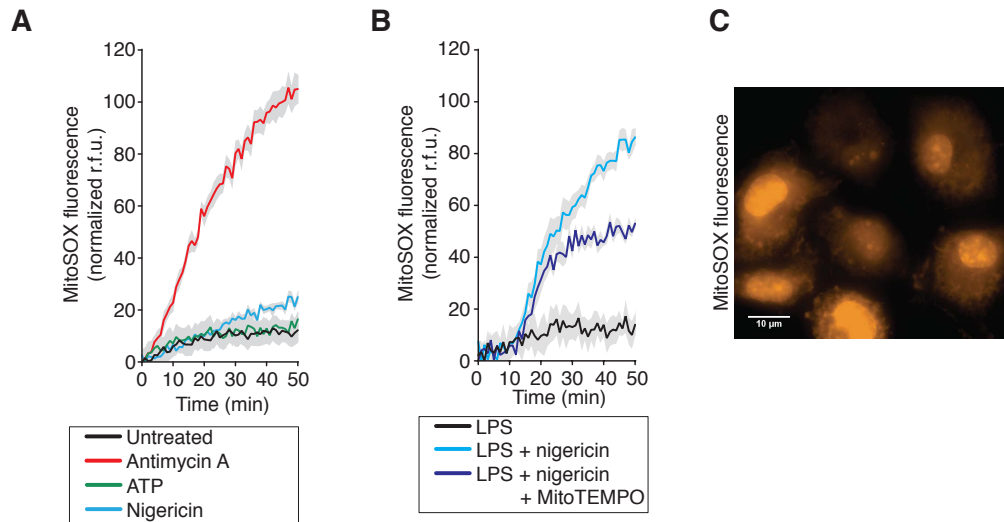




- A, B Different macrophage genotypes (as indicated) were primed for 4 h with LPS (10 ng/ml) and then stimulated for 20 min with ATP (3 mM) or nigericin (5  $\mu$ M). IL-1 $\beta$  (A) or LDH (B) were detected in the cell-free supernatants.
- C Immunoblot for TOMM20 and  $\alpha$ -tubulin in cytosolic enriched fraction and organelle enriched fraction obtained from different macrophage genotypes (as indicated) primed and activated as in A.
- D Immunoblot for TOMM20, GSDMD and  $\alpha$ -tubulin in cell lysates and mitochondria fraction obtained from wild type macrophages primed and activated as in A. Mitochondrial fraction was isolated with ultracentrifugation.
- E Immunoblot for TOMM20, GSDMD and  $\alpha$ -tubulin in cell lysates and mitochondria fraction obtained from wild type macrophages primed as in A and then stimulated with nigericin (10  $\mu$ M). Mitochondrial fraction was isolated with an antibody-based kit.
- F Different genotypes of macrophages (as indicated) were primed and activated as in A. Maximum intensity projections of z-stack images of macrophages stained with TOMM20 antibodies (green) and DAPI (blue) are shown. Scale bar represents 8  $\mu$ m.

Data information: Data in panel A and B are means  $\pm$  SEM from at least ten independent experiments. Statistical analyses were performed using non-parametric Mann–Whitney t-tests. Data were considered significant when \*\*\*P < 0.001. Immunoblots in panels C, D and E are from  $n=1$  independent experiment. Microscopy images in panel F are representative of three independent experiments.

## Supplementary Figure S2

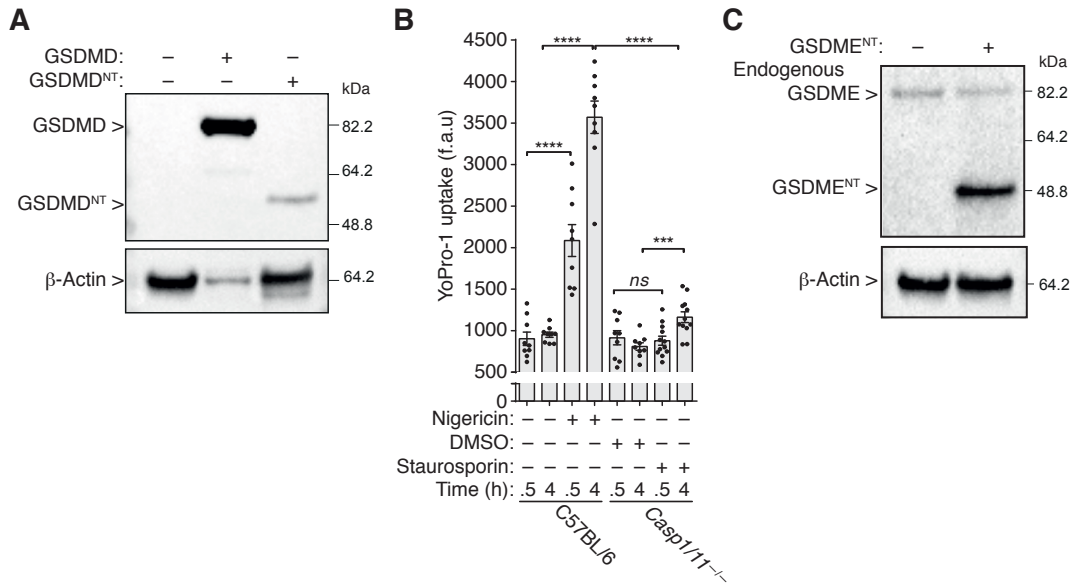


### Supplementary Figure S2. MitoTEMPO partially blocks MitoSOX fluorescence

- A Kinetic of MitoSOX fluorescence of unprimed wild type macrophages stimulated with ATP (3 mM), nigericin (5 μM) or antimycin A (10 μM).
- B Kinetic of MitoSOX fluorescence of macrophages primed for 4 h with LPS (10 ng/ml) and then stimulated with nigericin (5 μM) in presence or absence of MitoTEMPO (250 mM). Cells treated with inhibitors were incubated 10 min before and during stimulation of the cells.
- C Images of macrophages stained with MitoSOX. Scale bar represents 10 μm.

Data information: Data are means ± SEM from at least three independent experiments. Microscopy image of panel B is representative of 2 independent experiments.

## Supplementary Figure S3

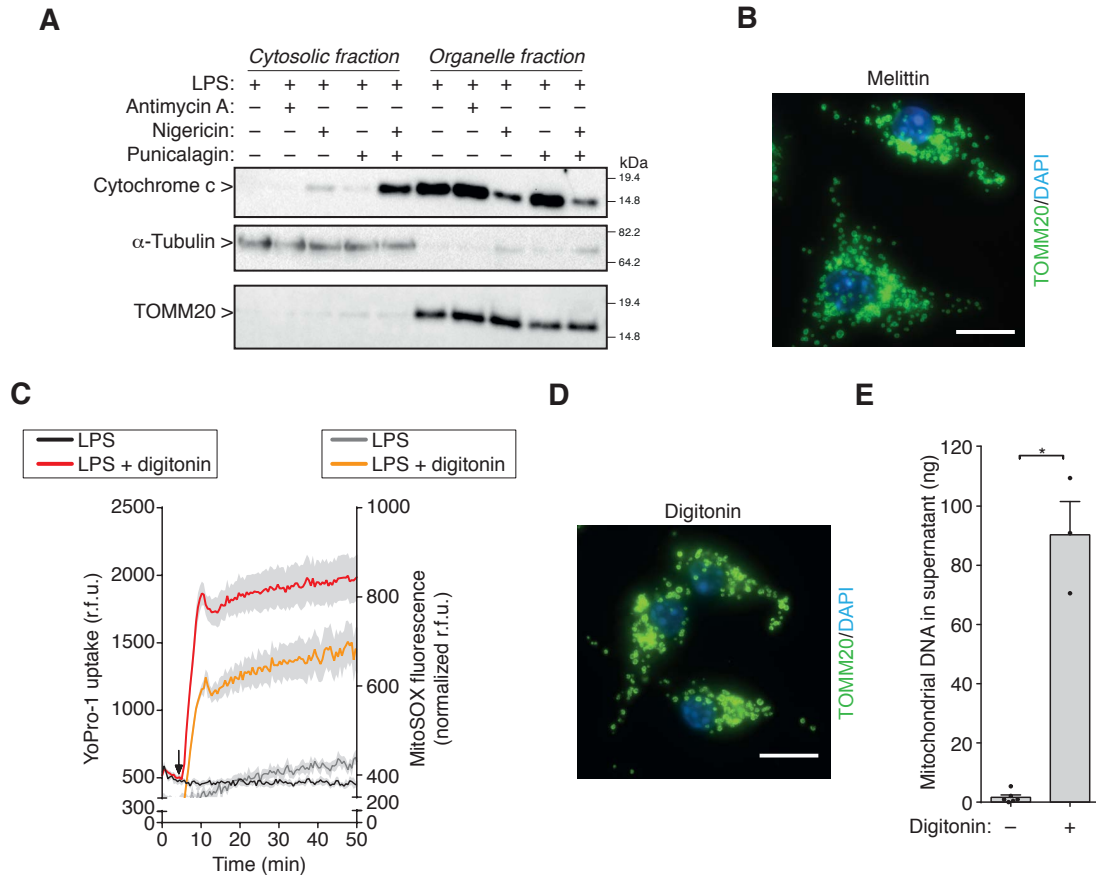


### Supplementary Figure S3. GSDMD<sup>NT</sup> and GSDME<sup>NT</sup> expression

- A** Immunoblot for Flag (GSDMD and GSDMD<sup>NT</sup>) and β-Actin in cell lysates of HEK293T transfected for 12 h with a plasmid encoding human GSDMD or human GSDMD<sup>NT</sup> (1-275).
- B** YoPro-1 uptake of wild type macrophages primed for 4 h with LPS (10 ng/ml) and stimulated with nigericin (10 μM), or *Casp1/11*<sup>-/-</sup> macrophages treated with DMSO or staurosporin (1 μM). YoPro-1 fluorescence was measured at the indicated times.
- C** Immunoblot for GSDME and β-Actin in cell lysates of HEK293T transfected for 12 h with a plasmid encoding for human GSDME<sup>NT</sup> (1-270) or with a control empty vector (pcDNA).

Data information: Immunoblots in panels A and C are representative of three independent experiments. Data in panel B are means ± SEM from three-four independent experiments in triplicates. Statistical analyses were performed using non-parametric Mann-Whitney t-tests. Data were considered significant when \*\*\*P < 0.001 or \*\*\*\*P < 0.0001

## Supplementary Figure S4



### Supplementary Figure S4. Plasma membrane permeabilization induces mitochondrial network fragmentation

- A** Immunoblot for cytochrome c, TOMM20 and  $\alpha$ -tubulin in cytosolic enriched fraction and organelle enriched fraction obtained from macrophages primed for 4 h with LPS (10 ng/ml) and then treated for 20 min with nigericin (5  $\mu$ M) or antimycin A (10  $\mu$ M), in the presence or absence of punicalagin (25  $\mu$ M).
- B** Maximum intensity projections of z-stack images of *Casp1/11<sup>-/-</sup>* macrophages treated as in A and stained with TOMM20 antibodies (green) and DAPI (blue). Scale bar represents 10  $\mu$ m.
- C** Kinetic of MitoSOX fluorescence and YoPro-1 uptake in wild type macrophages primed for 4 h with LPS (10 ng/ml) and then treated with digitonin (50  $\mu$ g/ml) when indicate by the arrow
- D** Maximum intensity projections of z-stack images of wild type macrophages treated as in C and stained with TOMM20 antibodies (green) and DAPI (blue). Scale bar represents 10  $\mu$ m.
- E** Mitochondrial DNA presence in cell-free supernatants from macrophages primed and stimulated as in C.

Data information: Immunoblots in panel A are from  $n= 1$  experiments. Microscopy image in panel B is representative of 3 independent experiments. Data in panel C are means  $\pm$  SEM from three independent experiments. Microscopy image of panel D is representative of three independent experiments. Data in panel E are means  $\pm$  SEM from 3 independent experiments. Statistical analyses were performed using non-parametric Mann–Whitney t-tests. Data were considered significant when  $*P < 0.05$ .